

Computing exact moments of local random quantum circuits via tensor networks

Paolo Braccia,¹ Pablo Bermejo,^{2,3} Lukasz Cincio,¹ and M. Cerezo^{2,*}

¹*Theoretical Division, Los Alamos National Laboratory, Los Alamos, NM 87545, USA*

²*Information Sciences, Los Alamos National Laboratory, Los Alamos, NM 87545, USA*

³*Donostia International Physics Center, Paseo Manuel de Lardizabal 4, E-20018 San Sebastián, Spain*

A basic primitive in quantum information is the computation of the moments $\mathbb{E}_U[\text{Tr}[U\rho U^\dagger O]^t]$. These describe the distribution of expectation values obtained by sending a state ρ through a random unitary U , sampled from some distribution, and measuring the observable O . While the exact calculation of these moments is generally hard, if U is composed of local random gates, one can estimate $\mathbb{E}_U[\text{Tr}[U\rho U^\dagger O]^t]$ by performing Monte Carlo simulations of a Markov chain-like process. However, this approach can require a prohibitively large number of samples, or suffer from the sign problem. In this work, we instead propose to estimate the moments via tensor networks, where the local gates moment operators are mapped to small dimensional tensors acting on their local commutant bases. By leveraging representation theoretical tools, we study the local tensor dimension and we provide bounds for the bond dimension of the matrix product states arising from deep circuits. We compare our techniques against Monte Carlo simulations, showing that we can significantly out-perform them. Then, we showcase how tensor networks can exactly compute the second moment when U is a quantum neural network acting on thousands of qubits and having thousands of gates. To finish, we numerically study the anticoncentration phenomena of circuits with orthogonal random gates, a task which cannot be studied via Monte Carlo due to sign problems.

I. INTRODUCTION

Computing the moments of expectation values measured at the output of random quantum circuits has become an important task in quantum information sciences. For instance, their analysis can help us determine conditions leading to non-classical simulability and exponential quantum advantage [1–6], the onset of quantum chaos [7–9], and the presence of local minima and barren plateaus in variational quantum computing [10–21]. When the circuit is sampled from a compact unitary group, one can leverage tools from Weingarten calculus [22, 23] to exactly evaluate these moments, even being able to compute them asymptotically [24]. However, if the unitaries U are sampled from a generic distribution, the calculation quickly becomes extremely hard and intractable.

To make the problem more manageable, researchers have studied circuits which have additional structure to them. One of the most physically motivated assumptions is that U is composed of local Haar random gates [8, 9, 25–29]. In this framework, one can map the problem of computing the moment to a Markov chain-like process, which enables the use of tools from classical statistical mechanics [9, 13, 17, 30–33]. This approach has shown to be incredibly successful, and it particularly excels at producing upper and lower bounds for the moments. However, there

is still room for improvement. In particular, for most of the aforementioned techniques to work, it is not always sufficient to consider that the unitary is composed of local random gates, as other assumptions are usually needed. For instance, one could require that the gates are sampled from the same group, or that the circuit gates have either a very regular arrangement or a very random one. Moreover, one could also be interested in computing the exact value of the moments, and not their bound. While some of these limitations can be overcome by using Monte Carlo (MC) sampling of the Markov chain-like process [13], this approach can still require a prohibitively large number of samples due to its additive error, or suffer from the sign problem [34, 35].

In this work we propose using Tensor Networks (TN) to compute the moments of the random quantum circuit’s expectation values. At its core, our work leverages the vectorization picture to represent the circuit’s initial state and the measurement operator t -th fold products as Matrix Product State (MPS) [36, 37] and the local unitaries moment matrices as gates arising from the projectors between their local commutants (see Fig. 1). This formalism is quite flexible, being applicable to general gate topologies, as well as circuits where the local gates are sampled from different groups. Of course, we are not claiming that the tensor contractions will always be efficient, since their difficulty will depend on several factors such as the gate’s topology, and the local dimensions of the tensors. Still, our approach has several advantages over MC techniques. For example TNs do not suffer from sign problems, nor require

* cerezo@lanl.gov

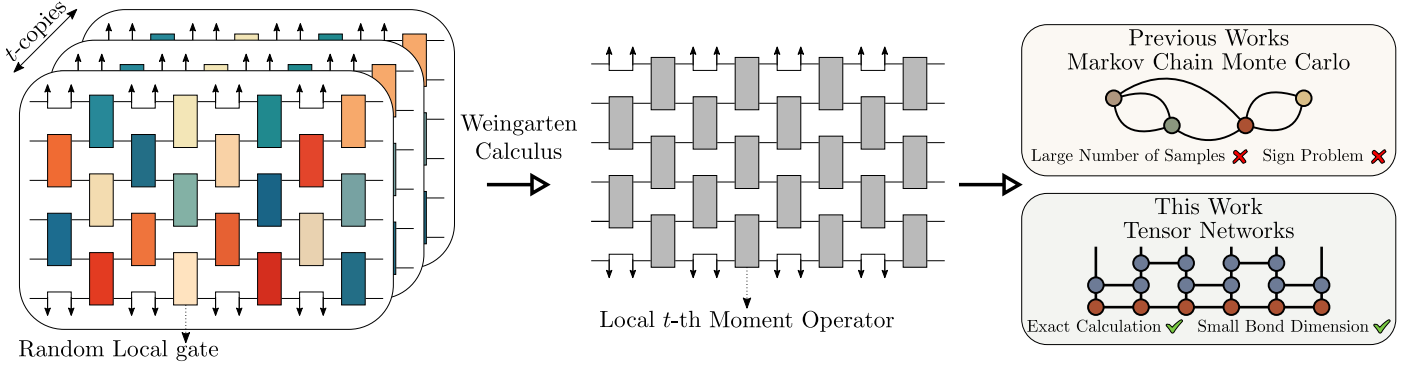


Figure 1. Schematic representation of our main results. Our ultimate goal is to estimate expectation values of the form $\mathbb{E}_U[\text{Tr}[U\rho U^\dagger O]^t]$, where ρ is a quantum state, U a quantum circuit composed of local random gates, and O some observable. By leveraging tools from the Weingarten calculus we can map this problem to that of evaluating the inner product $\mathbb{E}_U[\text{Tr}[V\rho V^\dagger O]^t] = \langle\langle \rho^{\otimes t} | \hat{\tau}^{(t)} | O^{\otimes t} \rangle\rangle$, where $|\rho^{\otimes t}\rangle$ and $|O^{\otimes t}\rangle$ are respectively the vectorized t -th fold tensor product of the initial state and measurement, and where $\hat{\tau}^{(t)}$ is the product of the local gates t -th moment operators. Previous works have proposed to compute this inner product by interpreting $\hat{\tau}^{(t)}$ as a Markov chain-like process and using MC sampling techniques. In this work, we instead evaluate this quantity by expressing $|\rho^{\otimes t}\rangle$ and $|O^{\otimes t}\rangle$ as MPSs, and $\hat{\tau}^{(t)}$ as a TN with local gates.

sampling. In addition, we also make theoretical contributions by leveraging tools from representation theory to compute the local dimension of the TNs, as well as provide bounds for the maximum bond dimension of MPSs arising from deep circuits. Moreover, we showcase our methods by comparing them against MC sampling, revealing that we can indeed compute the moments with much higher precision when using TN. We then present large scale numerical experiments which illustrate the power of TNs for studying the variance of expectation value. Finally, we show that having access to the MPSs representation of the initial state (or measurement) as it evolves through the TN moment gates enables a new dimension of analysis, such as the study of this vector's entropic properties.

II. FRAMEWORK

In what follows we will consider a random unitary quantum circuit U acting on an n -qudit Hilbert space $\mathcal{H} = (\mathbb{C}^d)^{\otimes n}$. We further assume that the circuit takes the form $U = \prod_{l=1}^L U_{\gamma_l}$, i.e., that it is composed of L local gates acting on $k_l \leq k$ qudits according to some topology $\mathcal{T} = \{\gamma_l\}_{l=1}^L$. Here, each $\gamma_l \in [n]^{\otimes k_l}$ is a tuple of (non-repeating) k_l indexes ranging between 1 and n which determine the set of qubits that U_{γ_l} acts on. For instance, if the circuit is a one-dimensional ansatz acting on alternating pairs of qudits (see Fig. 1), then we would have $\mathcal{T} = \{(1, 2), (3, 4), \dots, (n-1, n), (2, 3), \dots\}$. Moreover, we will assume that each U_{γ_l} belongs to some unitary Lie

group $G_l \subseteq U(d^{k_l})$.

Next, we will focus on studying moments of expectation values of the form

$$\ell_U(\rho, O) = \text{Tr}[U\rho U^\dagger O], \quad (1)$$

which correspond to sending an input n -qudit state ρ through U and measuring the expectation value of a Hermitian observable O at the circuit's output. Here, by moments we mean analyzing quantities such as

$$\mathbb{E}_U[\ell_U(\rho, O)], \quad \mathbb{E}_U[(\ell_U(\rho, O))^2], \quad (2)$$

or more generally $\mathbb{E}_U[(\ell_U(\rho, O))^t]$ ¹ for some $t \in \mathbb{N}$. In the previous, the expectation value is taken over the set of unitaries obtained by sampling each local U_{γ_l} independently and identically distributed (i.i.d.) according to the Haar measure $d\mu$ over G_l . As such, we can express $\mathbb{E}_U = \mathbb{E}_{G_L} \cdots \mathbb{E}_{G_1}$, with $\mathbb{E}_G[f(U)] = \int_G d\mu(U)f(U)$ the Haar integral over the group G .

III. CONNECTION TO THE LITERATURE

Before proceeding to the description of our results, we find it important to compare our methods with other techniques that exist in the literature. In particular, given the

¹ We note that while not explicitly stated, our methods can be trivially extended to compute more general moments such as $\mathbb{E}_U[\prod_{\eta=1}^t \text{Tr}[U\rho_\eta U^\dagger O_\eta]]$.

pervasiveness of quantities such as those in Eq. (2), their computation has received considerable attention. The simplest approach to computing these expectation values is by running the circuit N times (sampling random local unitaries each time) and computing the sample mean of the set of observations. While such approach is by far the simplest, it has the significant –and often overlooked– disadvantage that the ensuing expectation values come with a statistical uncertainty of $1/\sqrt{N}$. As such, computing the moments to a large precision requires a large number of circuit repetitions.

A more principled theoretical approach to computing the values in Eq. (2) has been taken in [4, 11–13, 17, 30–32] where the authors leverage tools from Weingarten calculus to analytically compute averages over each local Haar random gate. As further detailed below, the previous approach maps the problem of evaluating $\mathbb{E}_U[(\ell_U(\rho, O))^t]$ to a Markov chain-like problem, therefore enabling the use of classical statistical mechanics [4, 9, 13, 30, 32, 33]. In particular, these works consider exclusively circuits where all the local unitaries are sampled i.i.d. from the same fundamental representation of a unitary group, and where the circuit’s topology is somewhat structured. Moreover, their goal is to ultimately provide *upper and lower bounds* for the expectation value’s moments.

It is also important to note that for most cases considered in the literature, e.g., the expectation values with $t = 1$ and $t = 2$ as in Eq. (2), one can use MC methods to approximate the expectation values through the ensuing Markov chain-like approach [13]. While MC techniques can lead to good approximations of the moments, they have two critical issues. First, one needs to run the MC sampling algorithm a finite number of times, leading to an additive error. Since the expectation values $\mathbb{E}_U[(\ell_U(\rho, O))^t]$ can be exponentially small quantities, one could require a prohibitively large number of samples for their approximation. Second, and most importantly, the weights of the configuration can be negative, meaning that one can encounter the sign problem, which increases exponentially the computational complexity of the MC simulation [34, 35].

In this work, we will follow a similar approach to the one in [4, 11–13, 17, 30–32], as we make use of Weingarten to map the problem of calculating $\mathbb{E}_U[(\ell_U(\rho, O))^t]$ to that of evolving a state through a Markov chain-like process matrix. However, unlike previous approaches which leverage statistical mechanics or MC simulations, we will here present a TN method which allows us to exactly obtain the expectation values. Our techniques can be applied under quite general conditions, including the case when the local unitaries are sampled from subgroups of the unitary (such as the orthogonal group) and combinations thereof, as well as when the circuit topology is arbitrary. Moreover, as we

explicitly show in our numerical experiments section, the TN techniques introduced here can be employed in situations where a sign problem would arise for MC techniques.

IV. FROM WEINGARTEN CALCULUS TO TENSOR NETWORKS

A. Basics of Weingarten calculus

To begin, we recall a few basic concepts from Weingarten calculus. We refer the interested reader to [22–24] for a modern and detailed description of the tools used here.

Given a compact unitary Lie group G with Haar measure $d\mu$ acting on a finite-dimensional Hilbert space \mathcal{H} , we define the t -th fold twirl map $\tau_G^{(t)} : \mathcal{B}(\mathcal{H}^{\otimes t}) \rightarrow \mathcal{B}(\mathcal{H}^{\otimes t})$ as

$$\tau_G^{(t)}(X) = \int_G d\mu(V) V^{\otimes t} X (V^\dagger)^{\otimes t}, \quad (3)$$

for any $X \in \mathcal{B}(\mathcal{H}^{\otimes t})$. Here \mathcal{B} denotes the set of bounded operators acting on a given vector space. The importance of the twirl spans from the fact that any expectation value of the form $\mathbb{E}_G[\text{Tr}[V\rho V^\dagger O]^t]$ can be written as

$$\mathbb{E}_G \left[\text{Tr} \left[V\rho V^\dagger O \right]^t \right] = \text{Tr} \left[\tau_G^{(t)}(\rho^{\otimes t}) O^{\otimes t} \right] = \text{Tr} \left[\rho^{\otimes t} \tau_G^{(t)}(O^{\otimes t}) \right],$$

where we have used the linearity of the trace and the invariance of the Haar measure.

Then, we find it convenient to recall the vectorization formalism, in which an operator in $\mathcal{B}(\mathcal{H}^{\otimes t})$ is mapped to a vector in $\mathcal{H}^{\otimes t} \otimes (\mathcal{H}^*)^{\otimes t}$ while a channel from $\mathcal{B}(\mathcal{H}^{\otimes t})$ to $\mathcal{B}(\mathcal{H}^{\otimes t})$ is mapped to a matrix in $\mathcal{B}(\mathcal{H}^{\otimes t} \otimes (\mathcal{H}^*)^{\otimes t})$. Specifically, given some operator $X = \sum_{i,j=1}^{d^t} c_{ij} |i\rangle\langle j|$, its vectorized form is $|X\rangle\rangle = \sum_{i,j=1}^{d^t} c_{ij} |i\rangle \otimes |j\rangle$, while given a channel $\Phi(X) = \sum_{\nu=1}^{d^{2t}} K_\nu X J_\nu^\dagger$, we obtain $\hat{\Phi} = \sum_{\nu=1}^{d^{2t}} K_\nu \otimes J_\nu^*$. In this picture, we can verify that since $\langle\langle Y | \hat{\Phi} | X \rangle\rangle = \text{Tr}[Y^\dagger \Phi(X)]$, then

$$\mathbb{E}_G \left[\text{Tr} \left[V\rho V^\dagger O \right]^t \right] = \langle\langle \rho^{\otimes t} | \hat{\tau}_G^{(t)} | O^{\otimes t} \rangle\rangle, \quad (4)$$

where the Hermitian operator $\hat{\tau}_G^{(t)} \in \mathcal{B}(\mathcal{H}^{\otimes t} \otimes (\mathcal{H}^*)^{\otimes t})$, defined as

$$\hat{\tau}_G^{(t)} = \int_G d\mu(V) V^{\otimes t} \otimes (V^*)^{\otimes t} \quad (5)$$

is known as the t -th moment operator.

It is well known that the twirl map is a projection onto the t -th order commutant of G , i.e., the operator vector

space $\text{comm}^{(t)}(G) = \{M \in \mathcal{B}(\mathcal{H}^{\otimes t}) \mid [M, V^{\otimes t}] = 0\}$, of dimension $d_{G,t} = \dim(\text{comm}^{(t)}(G))$. As such, given a basis $\{P_\mu\}_{\mu=1}^{d_{G,t}}$ of $\text{comm}^{(t)}(G)$, one can express the twirl operator as

$$\tau_G^{(t)}(X) = \sum_{\mu,\nu=1}^{d_{G,t}} (W_{G,t}^{-1})_{\nu\mu} \text{Tr}[P_\mu X] P_\nu. \quad (6)$$

Here $W_{G,t}^{-1}$ is known as the Weingarten Matrix, and is the inverse² of the Gram matrix W of the commutant's basis (under the Hilbert-Schmidt inner product). That is, $W_{G,t}$ is a matrix with entries $(W_{G,t})_{\nu\mu} = \text{Tr}[B_\nu^\dagger B_\mu]$. In the vectorization picture, we have that

$$\hat{\tau}_G^{(t)} = \sum_{\mu,\nu=1}^{d_{G,t}} (W_{G,t}^{-1})_{\nu\mu} |P_\nu\rangle\rangle\langle\langle P_\mu|. \quad (7)$$

As a sanity check, one can verify that combining Eqs. (4) and (7) clearly recovers (6).

B. Mapping to a tensor network problem

Using the previous tools and techniques, we can thus express

$$\begin{aligned} \mathbb{E}_U[(\ell_U(\rho, O))^t] &= \langle\langle \rho^{\otimes t} | \prod_{l=1}^L \hat{\tau}_{G_l}^{(t)} | O^{\otimes t} \rangle\rangle \quad (8) \\ &= \langle\langle \rho^{\otimes t} | \hat{\tau}^{(t)} | O^{\otimes t} \rangle\rangle. \quad (9) \end{aligned}$$

where we defined $\hat{\tau}^{(t)} = \prod_{l=1}^L \hat{\tau}_{G_l}^{(t)}$. Equation (8) shows that in order to compute the expectation value, we need to compute the inner product between two vectors ($|\rho^{\otimes t}\rangle\rangle$ and $|O^{\otimes t}\rangle\rangle$) and the $d^{2tn} \times d^{2tn}$ matrix $\hat{\tau}^{(t)}$. Clearly, the evaluation of this expectation value becomes rapidly intractable as its dimension increases exponentially with the number of qudits n , and the moment's order t . However, since the gates are local, it is completely unnecessary to work with such large matrices, and the problem's dimension can be reduced to a much smaller problem size [4, 13].

To understand the previous let us note that $\hat{\tau}^{(t)}$ is a product of the local moment superoperators for each gate. Then, we can see by explicitly expanding the product of two adjacent moment operators that

$$\begin{aligned} \hat{\tau}_{G_{l+1}}^{(t)} \hat{\tau}_{G_l}^{(t)} &= \sum_{\mu_{l+1}, \nu_{l+1}} \sum_{\mu_l, \nu_l} (W_{G_{l+1},t}^{-1})_{\nu_{l+1}\mu_{l+1}} (W_{G_{l+1},t}^{-1})_{\mu_{l+1}\nu_{l+1}} \\ &\quad \times |P_{\nu_{l+1}}\rangle\rangle\langle\langle P_{\mu_{l+1}}| P_{\nu_l}\rangle\rangle\langle\langle P_{\mu_l}|. \end{aligned}$$

² Or pseudo-inverse if W is singular.

That is, the product of two moment operators can be understood as a map between the basis elements of the t -th order commutant of the first gate, to that of the last gate. As such, we can attempt to find a more efficient representation of the $\hat{\tau}_{G_l}^{(t)}$ projectors as a process matrix in the bases arising from the local commutants. In turn, such representation will map $\hat{\tau}^{(t)}$ to a sequence of L such process matrices arranged according to the topology of \mathcal{T} which we can then interpret as a circuit's TN. Then, if we represent $|\rho^{\otimes t}\rangle\rangle$, and $|O^{\otimes t}\rangle\rangle$ as MPSs in the aforementioned commutants' bases, the expectation value $\mathbb{E}_U[(\ell_U(\rho, O))^t]$ in Eq. (8) can be computed via standard TNs techniques. As previously mentioned, and as exemplified in our numerics section, having access to the MPS representation of $\hat{\tau}^{(t)}|O^{\otimes t}\rangle\rangle$ opens up a whole new dimension of analysis, given that we can study its entropic properties as it evolved through the TN gates. Notably, such analysis is readily available from our TN approach, but is not accessible via MC sampling techniques, thus further differentiating our work from previous literature.

C. Toy model example

To illustrate the previous idea of tackling the problem via TNs, consider an $n = 3$ qubit system ($d = 2$) where the random quantum circuit is composed of two ($L = 2$) two-qubit gates ($k_l = 2$ for $l = 1, 2$) following the topology $\mathcal{T} = \{(1, 2), (2, 3)\}$ (see Fig. 2(a)). That is

$$U = \prod_{l=1}^2 U_{\gamma_l} = U_{(2,3)} U_{(1,2)}. \quad (10)$$

Then, let us assume that both local unitaries are sampled i.i.d. from the fundamental representation of $U(4)$. Moreover, we will be interested in evaluating the second moment $\mathbb{E}_U[(\ell_U(\rho, O))^2]$. To finish, let us denote the Hilbert space over which U acts as $\mathcal{H} = \mathcal{H}_1 \otimes \mathcal{H}_2$, where \mathcal{H}_j is the Hilbert space of the j -th qubit.

It is well known that

$$\text{comm}^{(2)}(G) = \text{span}_{\mathbb{C}}\{\mathbb{1} \otimes \mathbb{1}, \text{SWAP}\}, \quad (11)$$

where $\mathbb{1}$ denotes the identity matrix acting on \mathcal{H} , while SWAP is the operator that exchanges the two copies of the (two-qubit) Hilbert space [22, 23, 38]. Since the operators in this basis are non-normalized and non-orthogonal, we find it convenient to instead define the orthonormal basis (under the Hilbert-Schmidt inner product)

$$\text{comm}^{(2)}(G) = \text{span}_{\mathbb{C}} \left\{ \frac{\mathbb{1} \otimes \mathbb{1}}{4}, \frac{\text{S} \otimes \mathbb{1} + \mathbb{1} \otimes \text{S} + \text{S} \otimes \text{S}}{4\sqrt{15}} \right\}.$$

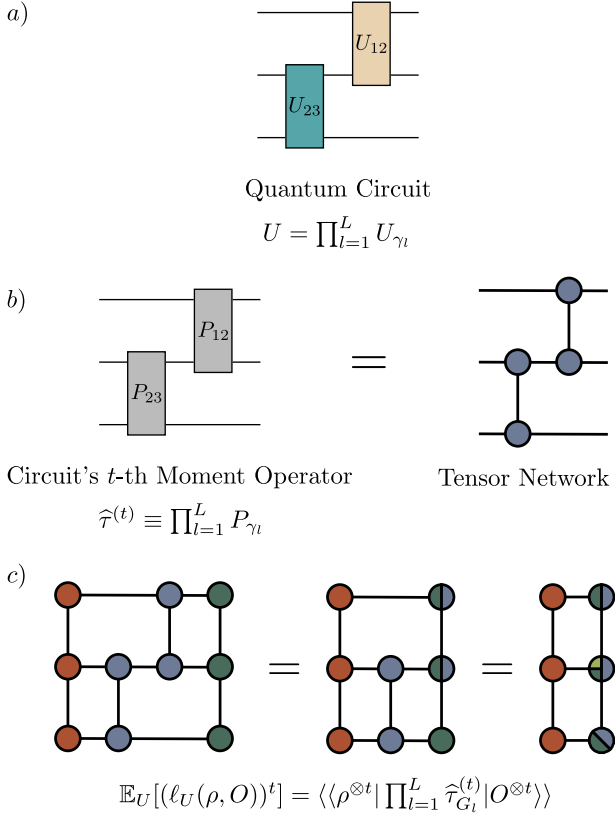


Figure 2. a) We consider a quantum circuit composed of L local random gates arranged according to some topology \mathcal{T} , and acting on an n -qudit system. b) The TN for the ensuing operator $\hat{\tau}^{(t)}$ will have n legs and will be composed of L gates arranged with the same topology \mathcal{T} . c) By expressing the vectorized operators $|\rho^{\otimes t}\rangle$ and $|O^{\otimes t}\rangle$ as MPSs, we can evaluate the moment by contracting these MPSs with the TN of $\hat{\tau}^{(t)}$.

Here, we have used the fact that we can always express $\text{SWAP} = \text{SWAP}_1 \otimes \text{SWAP}_2$, with SWAP_j the operator that swaps the j -th qubits, as well as the fact that

$$\text{SWAP} = \frac{1}{2} (\mathbb{1} + S),$$

with $S = X \otimes X + Y \otimes Y + Z \otimes Z$ and X, Y and Z the Pauli operators. Here we implicitly reordered the order of the Hilbert spaces from $\mathcal{H} \otimes \mathcal{H}$ to $\mathcal{H}_1^{\otimes 2} \otimes \mathcal{H}_2^{\otimes 2}$, so that SWAP_1 (SWAP_2) acts on the two copies of the first (second) qubit's Hilbert space.

With the previous, we can express the vectorized orthonormal basis of $\text{comm}^{(2)}(G)$ as

$$\left\{ \frac{|\mathbb{1}\rangle|\mathbb{1}\rangle}{4}, \frac{|\mathbb{S}\rangle|\mathbb{1}\rangle + |\mathbb{1}\rangle|\mathbb{S}\rangle + |\mathbb{S}\rangle|\mathbb{S}\rangle}{4\sqrt{15}} \right\}. \quad (12)$$

In this notation, one can verify that the following equalities hold

$$\begin{aligned} \hat{\tau}_{U(4)}^{(2)} |\mathbb{1}\rangle|\mathbb{1}\rangle &= |\mathbb{1}\rangle|\mathbb{1}\rangle, \\ \hat{\tau}_{U(4)}^{(2)} |\mathbb{S}\rangle|\mathbb{1}\rangle &= \frac{1}{5} (|\mathbb{S}\rangle|\mathbb{1}\rangle + |\mathbb{1}\rangle|\mathbb{S}\rangle + |\mathbb{S}\rangle|\mathbb{S}\rangle), \\ \hat{\tau}_{U(4)}^{(2)} |\mathbb{1}\rangle|\mathbb{S}\rangle &= \frac{1}{5} (|\mathbb{S}\rangle|\mathbb{1}\rangle + |\mathbb{1}\rangle|\mathbb{S}\rangle + |\mathbb{S}\rangle|\mathbb{S}\rangle), \\ \hat{\tau}_{U(4)}^{(2)} |\mathbb{S}\rangle|\mathbb{S}\rangle &= \frac{3}{5} (|\mathbb{S}\rangle|\mathbb{1}\rangle + |\mathbb{1}\rangle|\mathbb{S}\rangle + |\mathbb{S}\rangle|\mathbb{S}\rangle), \end{aligned}$$

meaning that we can represent the effective action of $\hat{\tau}_{U(4)}^{(2)}$ as the 4×4 matrix ($2 \times 2 \times 2 \times 2$ tensor)

$$\hat{\tau}_{U(4)}^{(2)} \equiv P = \begin{pmatrix} 1 & 0 & 0 & 0 \\ 0 & 1/5 & 1/5 & 3/5 \\ 0 & 1/5 & 1/5 & 3/5 \\ 0 & 1/5 & 1/5 & 3/5 \end{pmatrix}. \quad (13)$$

Importantly, P acts on two, two-dimensional, vector spaces with basis $\{|\mathbb{1}\rangle, |\mathbb{S}\rangle\}$.

From the previous, and as shown in Fig. 2(b), the product of these moment operators can be reduced to a 8×8 matrix (a $2 \times 2 \times 2 \times 2 \times 2 \times 2$ tensor)

$$\hat{\tau}^{(2)} \equiv P_{(2,3)} P_{(1,2)}, \quad (14)$$

where $P_{(2,3)}$ indicates that the P gate of Eq. (13) acts on the second and third two-dimensional legs. If we compare Eqs. (10) with (14), this example shows that the circuit's moment operator can be expressed as a TN composed of $2 \times 2 \times 2 \times 2$ tensors. Then, the expectation value $\mathbb{E}_U[(\ell_U(\rho, O))^2]$ in Eq. (8) can be estimated by representing $|\rho^{\otimes 2}\rangle$ and $|O^{\otimes 2}\rangle$ as an MPS in the basis $\{|\mathbb{1}\rangle, |\mathbb{S}\rangle\}^{\otimes 3}$, and evaluating the inner product of these smaller operators (see Fig. 2(c)). For instance if O is a Pauli operator on the first qubit, then

$$|O^{\otimes 2}\rangle \equiv \frac{1}{3} |\mathbb{S}\rangle|\mathbb{1}\rangle|\mathbb{1}\rangle, \quad (15)$$

which is an MPS of bond dimension $\chi = 1$. Here, we have exploited the fact that from the point of view of twirling over $U(4)$, every Pauli operator is the same, i.e., $\tau_{U(4)}^{(2)}(X_1^{\otimes 2}) = \tau_{U(4)}^{(2)}(Y_1^{\otimes 2}) = \tau_{U(4)}^{(2)}(Z_1^{\otimes 2}) = \frac{1}{3} \tau_{U(4)}^{(2)}(S)$.

D. General formalism

The previous example illustrates how $\mathbb{E}_U[(\ell_U(\rho, O))^t] = \langle \langle \rho^{\otimes t} | \hat{\tau}^{(t)} | O^{\otimes t} \rangle \rangle$ can be computed by representing $\hat{\tau}^{(t)}$ as an n -legged TN and $|\rho^{\otimes t}\rangle$ and $|O^{\otimes t}\rangle$ as MPSs. In fact,

just like in the previous toy model, given a unitary with random local gates of the form $U = \prod_{l=1}^L U_{\gamma_l}$, the TN for $\hat{\tau}^{(t)}$ will have n legs and will be composed of L gates –which we will dub “ P gates”– arranged according to the topology \mathcal{T} . That is

$$\hat{\tau}^{(t)} = \prod_{l=1}^L P_{\gamma_l}. \quad (16)$$

Each P_{γ_l} gate will have k_l legs, and its input and output dimensions will depend on who the local group G_l is, but also on the P gates that precede and follow it (as it needs to capture how the local commutants get projected into each other). In the simpler case when $k_l = k \forall l$ and when all the local groups are the same, the P gates will have the same dimensions.

Note that the previous does not imply that we can efficiently contract the tensors, as this will ultimately depend on the local tensor dimensions, the circuit topology, and the entanglement in the MPSs arising from the initial state and measurement operator. In what follows we present a few general considerations that will allow us to better understand when the TN simulation might be efficient.

We begin by analyzing the dimensions of the P gates. For instance, we can show that the follow result holds.

Theorem 1. *Let U be a random quantum circuit composed of L two-qudit gates. If the local unitaries are sampled i.i.d. from the fundamental representation of the Lie group $G \in \{U(d^k), O(d^k), Sp(d^k/2)\}$ (assuming d even), then the P gate for each $\hat{\tau}_{G_l}^{(t)}$ will be a square matrix of dimension up to $(t!)^2 \times (t!)^2$ for $G = U(d^k)$, and of dimension up to $\left(\frac{(2t!)}{2^{t!}}\right)^2 \times \left(\frac{(2t!)}{2^{t!}}\right)^2$, for $G = O(d^k), Sp(d^k/2)$.*

The proof of this theorem, as well as that of our other main theoretical results, can be found in the appendices.

For the special case of a circuit composed of two-qubit gates ($d = 2$ and $k = 2$), Theorem 1 implies that the first moment operator will be trivial for any $G \in \{U(d^k), O(d^k), Sp(d^k/2)\}$, as the P -gates for each $\hat{\tau}_{G_l}^{(1)}$ are one dimensional projectors onto the vectorized identity (which follows from the fact that the local groups are irreducible). Then, the second moment operator $\hat{\tau}^{(2)}$ will be composed of 4×4 square gates (or $2 \times 2 \times 2 \times 2$ tensors) for $G = U(4)$ given by Eq. (13), and of dimension 9×9 (or $3 \times 3 \times 3 \times 3$ tensors) for $G = O(4), Sp(2)$. We note that the dimension bounds given by Theorem 1 will be useful for small t or large qudit dimension d , but these can also be extremely loose. In this case, one can tighten them by using representation theoretical tools. For instance, if $d = 2$ and G is the unitary group, one should replace the upper

bound of $(t!)^2 \times (t!)^2$ by $(C_t)^2 \times (C_t)^2$, where C_t are the Catalan numbers³.

It is important to note that while the dimension of the tensor representation of $\hat{\tau}_{G_l}^{(t)}$ matches $(\dim(\text{comm}^{(t)}(G)))^2 \times (\dim(\text{comm}^{(t)}(G)))^2$ for these groups⁴, this is not a generic feature. In fact, the dimension of the $\hat{\tau}_{G_l}^{(t)}$ tensor can depend on who ρ and O are. For instance, if the unitary’s two-qubit gates are sampled from the free-fermionic reducible representation of $G = SO(4) \simeq SU(2) \oplus SU(2)$ [5, 16, 40–42], then we have that $\dim(\text{comm}^{(2)}(G)) = 10$ [16], which would imply that $\hat{\tau}_{G_l}^{(2)}$ are matrices of size 100×100 if one were to extrapolate the previous realization. However, we find that the following theorem holds.

Theorem 2. *Let U be random quantum circuit composed of L two-qubit gates. If the local unitaries are sampled i.i.d. from the free-fermionic reducible representation of the Lie group $G = SO(4) \simeq SU(2) \oplus SU(2)$ then the P gate for each $\hat{\tau}_{G_l}^{(t)}$ will be a square matrix of dimension 9×9 (or $3 \times 3 \times 3 \times 3$ tensors) if ρ has fixed parity, and of size 36×36 (or $6 \times 6 \times 6 \times 6$ tensors) if ρ is a generic state.*

Next, let us analyze the bond dimension of the MPSs arising from ρ and O . If ρ is a product state and if O can be expressed as a tensor product of Hermitian operators (e.g., a projector onto a computational basis state, or a Pauli operator), then $|\rho^{\otimes t}\rangle\rangle$ and $|O^{\otimes t}\rangle\rangle$ can be represented as MPSs with bond dimension $\chi = 1$. From here one can wonder how large the bond dimension of $\hat{\tau}^{(t)}|O^{\otimes t}\rangle\rangle$ or $\hat{\tau}^{(t)}|\rho^{\otimes t}\rangle\rangle$ will be as a function of the number of gates L in the circuit, and concomitantly of the P -gates in the TN. While the bond dimension for small L can vary widely depending on the local groups and topology (see the numerics section) we can make statements about the large L limit.

In particular, let us denote as G_U the Lie group to which the distribution of U converges to for large L . We can obtain G_U as follows. First, let $\mathcal{G}_l = \{iH_{lm}\}_{m=1}^{\dim(\mathfrak{g}_l)}$ be a basis for the Lie algebra \mathfrak{g}_l associated to the Lie group G_l

³ This follows from the fact that the order $t!$ of the symmetric group S_t can be much larger than the operator’s space dimension, leading to an over-complete basis. Here, one needs to instead compute how many trivial irreducible representations appear in the operator space decomposition under the adjoint action of the t -th fold representation.

⁴ Here we used the Schur-Weyl duality between the t -fold representation of the unitary group and the symmetric group S_t , as well as that for the t -th fold representation of the orthogonal (or symplectic) group and the Brauer algebra B_{2t} . See for instance [24, 39].

(that is $G_l = e^{\mathfrak{g}_l}$). Then, we need to compute the Lie algebra [43]

$$\mathfrak{g}_U = \left\langle \bigcup_{l=1}^L \mathfrak{G}_l \right\rangle_{\text{Lie}}, \quad (17)$$

where $\langle \cdot \rangle_{\text{Lie}}$ denotes the Lie closure, i.e., the vector space obtained by nested commutators of all the operators in the bases \mathfrak{G}_l . Such Lie algebra is important as $U \in G_U = e^{\mathfrak{g}_U}$ for any set of randomly sampled local gates. Moreover, as the number of gates increases, one can generally expect that $\mathbb{E}_U = \mathbb{E}_{G_L} \cdots \mathbb{E}_{G_1} \simeq \mathbb{E}_{G_U}$. The number of gates needed for the circuit to become a t -design over G_U can be estimated via the spectral gap of $\hat{\tau}^{(t)}$, i.e., how large its first not-equal-to-one eigenvalue is [14, 30, 32, 44–49].

The previous shows that if L is large enough so that the distribution of U becomes a t -design over G_U , then $\hat{\tau}^{(t)}$ becomes a projector onto $\text{comm}^{(t)}(G_U)$. Then, how large the bond dimension of $\hat{\tau}^{(t)}|O^{\otimes t}\rangle\rangle$ or $\hat{\tau}^{(t)}|\rho^{\otimes t}\rangle\rangle$ is will solely depend on what's the bond dimension of a linear combination of the vectorized operators in the basis of this commutant. Thus, we find that the following proposition holds.

Proposition 1. *Let U be deep enough so that it forms a 2-design over G_U . The bond dimension of the MPS $\hat{\tau}^{(t)}|A^{\otimes t}\rangle\rangle$ for any $A \in \mathcal{B}(\mathcal{H})$ is up to $\chi = t!$ for $G_U = U(d^n)$ and up to $\chi = \frac{(2t)!}{2^{t!}}$ for $G = O(d^n), Sp(d^n/2)$.*

When $t = 2$, Proposition 1 implies that irrespective of the number of qudits n , or the local dimension d , The maximum bond dimension of the MPS $\hat{\tau}^{(2)}|A^{\otimes 2}\rangle\rangle$ for any $A \in \mathcal{B}(\mathcal{H})$ is $\chi = 2$ for $G_U = U(d^n)$ and $\chi = 3$ for $G = O(d^n), Sp(d^n/2)$.

It is important to note that the results in the previous proposition follow from the fact that the elements in the commutants of $U(d^n), G = O(d^n), Sp(d^n/2)$ can be naturally expressed as rank-one projectors onto MPSs of bond dimension $\chi = 1$ for the Hilbert space $\mathcal{H}_1^{\otimes t} \otimes \mathcal{H}_2^{\otimes t} \cdots \otimes \mathcal{H}_n^{\otimes t}$, where \mathcal{H}_j denotes the Hilbert space of the j -th qudit. Such result will not generally hold, especially for the case when G_U is not an irreducible fundamental representation of a Lie group. In the more general scenario, one needs to find how the vectorized elements of $\text{comm}^{(t)}(G_U)$ will decompose in terms of operators acting on $\mathcal{H}_1^{\otimes t} \otimes \mathcal{H}_2^{\otimes t} \cdots \otimes \mathcal{H}_n^{\otimes t}$. Such analysis will be case by case dependent, but we can provide some guidelines for some special cases.

In particular, let us study the situation when $i\rho$ or iO belonging to \mathfrak{g}_U , and when $t = 2$. We recall that we can always express \mathfrak{g}_U in its reductive decomposition, i.e., as a direct sum of commuting ideals

$$\mathfrak{g}_U = \mathfrak{g}_1 \oplus \cdots \oplus \mathfrak{g}_{\zeta-1} \oplus \mathfrak{g}_{\zeta}, \quad (18)$$

where \mathfrak{g}_j are simple Lie algebras for $j = 1, \dots, \zeta - 1$, and with \mathfrak{g}_{ζ} being the center of \mathfrak{g}_U , and therefore abelian. Here, the only elements of the t -th fold commutant that will have non-zero overlap with $\rho^{\otimes 2}$ (or $O^{\otimes 2}$) are the Casimir operators $\{C_j\}_{j=1}^{\zeta}$ [14], where

$$C_j = \sum_{\mu=1}^{\dim(\mathfrak{g}_j)} B_{\mu} \otimes B_{\mu}, \quad (19)$$

and with $\{B_{\mu}\}_{\mu=1}^{\dim(\mathfrak{g}_j)}$ being an orthonormal basis for $i\mathfrak{g}_j$. For instance, we can use this insight to prove that

Proposition 2. *Let U be deep enough so that it forms a 2-design over the free-fermionic representation of $G_U = SO(2n)$, with associated Lie algebra $\mathfrak{g}_u = \mathfrak{so}(2n)$. Given some Pauli operator $A \in \mathcal{B}(\mathcal{H})$ such that $iA \in \mathfrak{g}_U$, then the maximum bond dimension of the MPS $\hat{\tau}^{(2)}|A^{\otimes 2}\rangle\rangle$ is $\chi = 3$.*

Propositions 1 and 2 show an interesting property of our proposed TN approach. In many cases, for shallow circuits with small L , the bond dimension of the MPS is generally small. This follows from the fact that the MPS representation of $|\rho^{\otimes t}\rangle\rangle$ and $|O^{\otimes t}\rangle\rangle$ can be such that $\chi = 1$, and since the gates in the circuit are local, they cannot generate too much entanglement. Then, for deep circuits with very large L the bond dimension of $\hat{\tau}^{(t)}|O^{\otimes t}\rangle\rangle$ (or $\hat{\tau}^{(t)}|\rho^{\otimes t}\rangle\rangle$) is small again.

V. DEALING WITH UNNORMALIZED TENSOR NETWORK CONTRACTIONS

The general formalism derived in the previous section allows us to compute t -th moment of an expectation value by building a tensor network. Here, one replaces the gates appearing in U with P tensors arising from the $\hat{\tau}_{G_l}^{(t)}$, and replaces local qudits Hilbert spaces \mathcal{H}_l with legs whose dimension depends on the local gate's commutants. For the sake of simplicity, we will refer to the resulting TN as the P -network, or P -net for short.

While this construction allows us to drastically reduce the dimension of the problem (see Theorems 1 and 2), care must be taken when dealing with the ensuing tensors, as neither the MPS encoding the (vectorized) t -th tensor product of the measurement operator $|O^{\otimes t}\rangle\rangle$ nor the one encoding the quantum state $|\rho^{\otimes t}\rangle\rangle$ are in principle normalized states. Similarly, the P -gates in the P -net need not be unitary (see for instance the P -gate in Eq. (13)). Hence, when evolving $|O^{\otimes t}\rangle\rangle$ (or $|\rho^{\otimes t}\rangle\rangle$) through the P -net, one could very quickly start facing very small or very large numbers, leading to loss of numerical precision or overflow

errors. In order to prevent such issues we propose the following recipe to contract the TN:

- We associate a vector \mathbf{n}_O to $|O^{\otimes t}\rangle$, whose length is equal to the size n of the system, and we fill it with ones. This vector will hold all the normalization factors of the measurement operator's MPS. After the application of P -gates acting in parallel, or after a given (fixed) number of gates in case of an unstructured topology, we perform a Singular Values Decomposition (SVD) sweep through $|O^{\otimes t}\rangle$, normalizing the singular values at each pair of sites. Namely, calling A_j^O the j -th tensor of the MPS $|O^{\otimes t}\rangle$, we contract adjacent tensors A_j^O, A_{j+1}^O , obtaining a two-sites tensor $\tilde{A}_{j,j+1}^O$ which we then decompose using SVD as, dropping super and subscripts for the sake of notation, $\tilde{A} = W_1 \cdot S \cdot W_2$, with W_1 and W_2 unitary tensors and S a diagonal matrix containing the singular values of \tilde{A} . We normalize $S \leftarrow S/\|S\|$, distributing the weight equally between W_1 and W_2 as $W_1 \leftarrow W_1\sqrt{S}$ and $W_2 \leftarrow \sqrt{S}W_2$ and update $A_j^O \leftarrow W_1$ and $A_{j+1}^O \leftarrow W_2$. In the process we also update the normalization factors as $(\mathbf{n}_O)_j \leftarrow (\mathbf{n}_O)_j\|S\|$, $(\mathbf{n}_O)_{j+1} \leftarrow (\mathbf{n}_O)_{j+1}\|S\|$. This procedure allows us to keep the norms of the tensors in ψ well-behaved.
- We associate an analogous vector \mathbf{n}_ρ to $|\rho^{\otimes t}\rangle$. We then normalize the tensors A_j^ρ to $\sqrt{\chi_j}$, χ_j being the bond dimensions of the link between sites j and $j+1$, and we save the normalization factors in \mathbf{n}_ρ as $(\mathbf{n}_\rho)_j = \|A_j^\rho\|/\sqrt{\chi_j}$. Notice that the last tensor will be normalized to one, as the non-existing link at the right of site n can be treated as having dimension $\chi_n = 1$. The intuition behind this is that if $|\rho^{\otimes t}\rangle$ were to be a normalized quantum state's MPS, in the left canonical form it would be composed of unitary tensors, whose norms are $\sqrt{\chi}$.
- Lastly, we compute the inner product $\langle\langle\rho^{\otimes t}|\hat{\tau}^{(t)}|O^{\otimes t}\rangle\rangle$ by initializing yet another vector \mathbf{n}_t and filling it with the norms of the sequential contractions of pairs of tensors A_j^O, A_j^ρ . Here, we start with the first tensors ($j = 1$), contract them, normalize the result, save the norm in $(\mathbf{n}_t)_1$, then proceed to contract this normalized tensor with the second tensors and so on.

Once all the tensor contractions have been performed we are left with three vectors $\mathbf{n}_O, \mathbf{n}_\rho, \mathbf{n}_t$. The overlap $\langle\langle\rho^{\otimes t}|\hat{\tau}^{(t)}|O^{\otimes t}\rangle\rangle$ is then obtained as the multiplication of all the entries of said vectors.

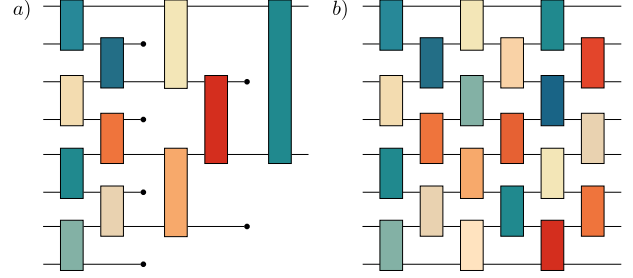


Figure 3. Circuit topologies for the numerical experiments. a) A QCNN is composed of a “convolutional” layer where two-qubit gates on act on alternating pairs of qubits, and of “pooling” layers, where half of the qubits are traced out. QCNNs naturally have a number of layers n_L in $\mathcal{O}(\log(n))$, and a number of local gates in $\mathcal{O}(n)$. b) In each layer of an HEA, gates act on alternating neighboring qubits in a brick-like fashion. Here we show an HEA with $n_L = 3$ layers with open boundary conditions. An HEA with n_L layer, has a number of gates in $\mathcal{O}(nm_L)$.

VI. NUMERICAL RESULTS

In this section, we showcase our TN framework by computing the exact $t = 2$ moments for two well-known qubit ($d = 2$) circuit topologies: a Quantum Convolutional Neural Networks (QCNN) [12, 50] and a one-dimensional Hardware Efficient Ansatz (HEA) [11, 51, 52], when all the gates composing U on each architecture are sampled i.i.d. first from the fundamental representations of $G = U(4)$ and from $G = O(4)$. The circuit topologies are shown in Fig. 3. Importantly, as we will see below, when the local gates are sampled from $O(4)$, MC simulations are not available due to a sign problem.

A. Local gates sampled from $G = U(4)$

In this section we will study the second moment for the case when O is a Pauli operator. However, instead of choosing a specific ρ , we will compute the inner product with all possible Paulis P_j in a basis of $\mathcal{B}(\mathbb{C}^{2^n})$ of bodyness $|P_j| = k$ (that is, P_j acts non trivially on k qubits). These quantities of interest will henceforth be called k -purities, denoted as $p_O^{(k)}$, and take the form

$$p_O^{(k)} = \frac{1}{4^n} \mathbb{E}_U \left[\sum_{P_j / |P_j|=k} \text{Tr}[P_j U^\dagger O U]^2 \right]. \quad (20)$$

It is not hard to see that since O is itself a Pauli, then $\sum_{k=1}^n p_O^{(k)} = 1$, and since by definition $p_O^{(k)} \geq 0$ for all k ,

then the k -purities form a probability distribution. Recalling that the first moment $\mathbb{E}_U \left[\sum_{P_j / |P_j|=k} \text{Tr}[P_j U^\dagger O U] \right] = 0$ for any non-identity Pauli (since the local group is irreducible, and its first order commutant trivial), we can interpret the collection of the k -purities as describing how the variance of the Heisenberg evolved operator $U^\dagger O U$ decomposes in terms of Paulis of a given bodyness.

As it was previously discussed, the core of our TN calculations rely on choosing an adequate basis for the local commutants, as these will define the gates for the P -net. For the case of $U(4)$, we have already derived in Eq. (13) the matrix representation of the P -gates for the particular choice of the local basis $\{|1\rangle\rangle, |S\rangle\rangle\}$.

1. Quantum convolutional neural network

We begin by taking U to be a QCNNS as introduced in [50]. To truly illustrate the power of our techniques, we consider a system of $n = 1264$ qubits. Clearly, a full density matrix simulation of the expectation values would be beyond any plausible supercomputer as it would require over 10^{1632} bits to save each amplitude to machine precision⁵.

In Fig. 4(blue), we show the k -purities of the QCNNS acting on $n = 1264$ qubits. Here, we can see that the vast majority of contributions to the k -purities are concentrated in a region with $k \sim n/3$. Moreover, it is clear that the distribution is skewed towards more local operators, and has essentially no contributions coming from global Paulis acting on all qubits. Of course, care must be taken when interpreting this result as we recall that it shows the cumulative purity for all Paulis of a given bodyness. If we wanted to ask: What is the contribution to the purity coming from a single Pauli acting on k -qubits, we would have to roughly divide $p_O^{(k)}$ by the number of Paulis $N_k = 3^k \binom{n}{k}$ of a given bodyness. Thus, since there are significantly more Paulis with bodyness $k = n/3$ than Paulis with bodyness $k = 1$ (see Fig. 4(orange)), we can expect that the contribution of a Pauli acting on a single-qubit must be much larger than that of a single Pauli acting on k qubits. In fact, we have shown in the inset of Fig. 4 the quantity $p_O^{(k)}/N_k$, and we can indeed see that the contributions to the purities decay exponentially with k .

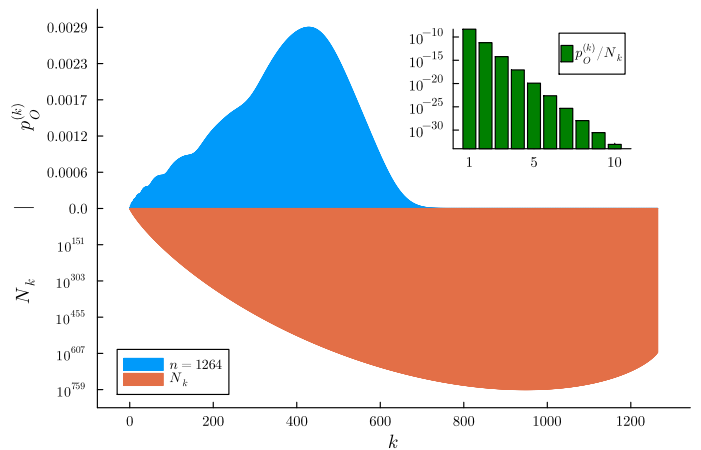


Figure 4. We show the distribution of k -purities of Eq. (20) for a QCNNS acting on $n = 1264$ qubits (blue). We also present the number of Paulis $N_k = 3^k \binom{n}{k}$ acting on k -qubits (orange). The inset depicts the quotient $p_O^{(k)}/N_k$.

2. One-dimensional hardware efficient ansatz

Let us now proceed to study the k -purities for an HEA acting on $n = 200$ qubits. In this example, the operator measured at the end of the circuit will be taken to be $O = Z_{n/2}$, Pauli- z operator acting on the middle qubit. Note that unlike the QCNNS where the number of layers is fixed, in an HEA, the depth of the circuit is a free parameter. As such, in Fig. 5 we show how the k -purities change as a function of the HEA's number of layers n_L . Here, we can see that –as expected due to the circuit's light-cone structure [11]– for shallow circuits $n_L = 1$ the Heisenberg evolved operator $U^\dagger O U$ is mostly local. This is evidenced from the fact that k -purities for $n_L = 1$ concentrate at $k \sim 2$. Then, as the number of layers increases, we can see that the distribution of k -purities shifts and peaks at higher values of k . Eventually, the distribution converges at an approximate Gaussian distribution with mean in $k \sim 3n/4$ (i.e., the purity distribution of $n_L = n/2$ and $n_L = n$ are completely indistinguishable). This is completely expected as it is known that one-dimensional hardware efficient ansatz with local random gates forms a 2-design over $SU(2^n)$ for $n_L \in \mathcal{O}(n)$ [32, 45, 46]. Such convergence is evidenced in our plots, and seen to be reached as early as $n_L = n/2$.

⁵ That is, we would need a device with over sixteen googol bits just for memory; or we would need to store ~ 20 bits of information in every atom of the visible universe.

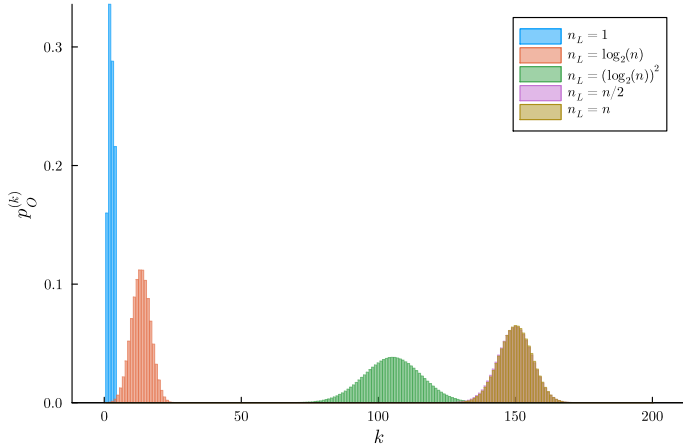


Figure 5. We show the distribution of k -purities of Eq. (20) for a one-dimensional HEA acting on $n = 200$ qubits as a function of the number of layers n_L . We note that the distributions for $n_L = n/2$ and $n_L = n$ are completely indistinguishable.

3. Maximum bond dimension scaling

The ability of our method to deal with QCNNS and deep HEAs acting on large number of qubits stems from the good behavior of the bond dimension χ of the MPS representing the evolution of the input measurement operator $|O^{\otimes t}\rangle$ throughout the P -net. In Fig. 6 we thus plot the maximum value χ_{\max} of the vectorized measurement operator MPS, different number of qubits n , and for different number of layers in U . For the QCNN, the max number of layers is $n_L = \lceil \log(n) \rceil$ (with $\lceil \cdot \rceil$ denoting the ceiling of a real-valued number), whereas for HEA we take $n_L = 1, \dots, n$. For a QCNN (Fig. 6(top)), we can see that the maximum bond dimension is always kept within reasonable levels (as further evidenced from the large scale numerics performed in Fig. (5)). Here, we can clearly see the effect of the ceiling in the number of layers, as when n surpasses a power of 2, the bond dimension exhibits small jumps. Then, for the HEA (Fig. 6(bottom)), we can surprisingly see that the bond dimension is always 4 irrespective of the number of qubits, and the number of layers. Both of these results show that our TN methods are well behaved and scalable for the circuit topologies considered.

4. Comparison with Monte Carlo techniques

As briefly discussed in the previous sections, a common approach in the literature to exactly estimate the $t = 1, 2$ moments is the use of MC sampling for the Markov chain-

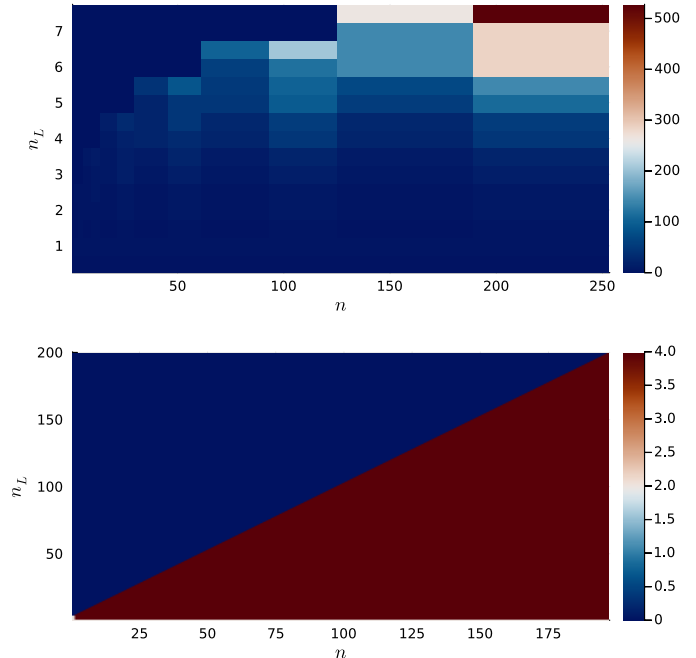


Figure 6. Scaling of the maximum bond dimension χ_{\max} of the MPS $|O^{\otimes t}\rangle$ for the QCNN circuit topology (top) and the HEA (bottom) as a function of the number of qubits n and the number of layers n_L .

like process [13]. To illustrate the advantage of our TN method versus MC sampling, we have implemented the algorithm in [13] to reconstruct the k -purity distribution via MC sampling for a QCNN and for an HEA, both with depth $n_L = \lceil \log(n) \rceil$. Denote as p_{tn} the ground-truth purity distribution obtained via our TN methods, and as p_{mc} the MC purity distribution. In Fig. 7 we plot the scaling of the Kullback-Leibler (KL) divergence $KL(p_{\text{tn}}, p_{\text{mc}}) = \sum p_{\text{tn}} \log(p_{\text{tn}}/p_{\text{mc}})$ between those two distributions, as the number of MC samples n_s increases from $n_s = 1$ to $n_s = 10^6$. As we can see in Fig. 7(top), when U is a QCNN, MC fails to accurately reproduce the purity distributions even at $n_s = 10^6$ samples. Moreover, we can see that as the number of qubits increases past a power of two, which implies an increase in the number of layers, the performance of MC decreases. In fact, as shown in the inset of this panel, at $n = 250$ qubits, an exponential increase in shots, leads to what appears to be a sub-linear improvement in the KL divergence. This fact implies that a supra-exponential number of MC samples might be needed to decrease the KL divergence by a constant amount. Then, as we can see in Fig. 7(bottom), for an HEA, while the KL

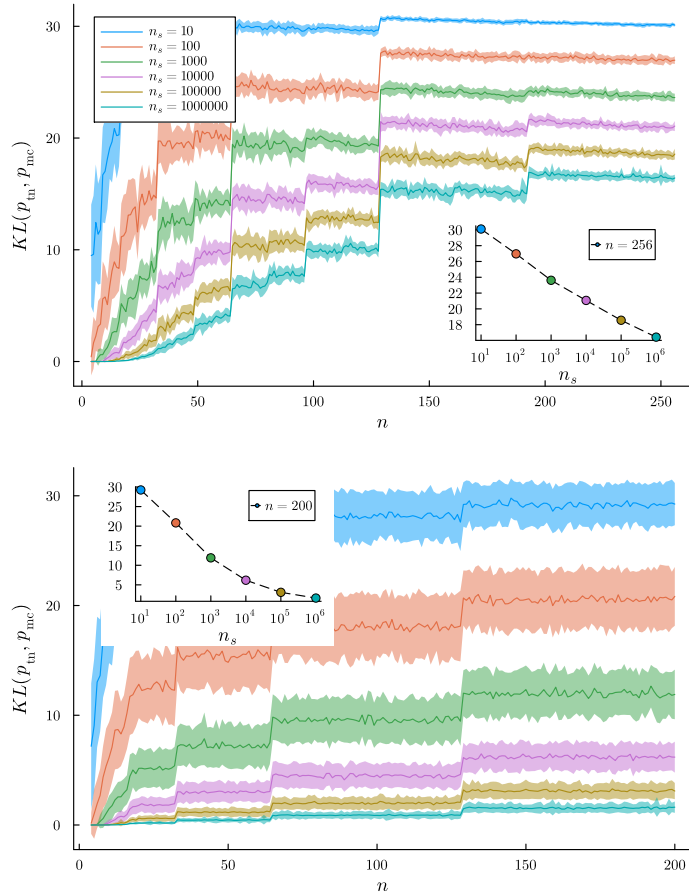


Figure 7. Scaling of Kullback-Leibler divergence between the purity distributions obtained via TNs (exact distribution) and via MC sampling for a QCNN (top) and an HEA (bottom) of different system sizes, and for different number n_s of MC samples. The curves show the average (solid line) and standard deviations (ribbon) over 100 independent MC runs. The insets show the decaying of the KL divergence at a fixed system size (largest n considered) as the number of MC samples increases.

divergence is smaller, indicating that MC can indeed lead to better purity distributions, the same phenomena occurs. Namely, exponentially increasing the number of measurements leads to smaller and smaller improvements in the KL divergence.

Taken together, these results show that our TN can significantly outperform standard MC sampling techniques.

5. Entanglement properties of the vectorized MPSs

In this section we showcase a novel dimension of analysis enabled from our TN approach. First, let us recall the (obvious) fact that as $|\mathcal{O}^{\otimes t}\rangle$ evolves through the gates of the P -net, it will always be an un-normalized vector in $\mathbb{R}^{\otimes n}$. As such, if we normalize it, we can consider that the MPS now represents a quantum state. Combining this realization with the fact that this MPS keeps a small bond dimension as it propagates through the layers of the P -net, allows for studying its entanglement and entropic properties.

Indeed, given a well-behaved MPS one can compute the entanglement properties of some reduced state [36, 37]. For instance, given a bipartition of the set of n MPS indexes as $\{I, \bar{I}\}$, we can compute the entropy of entanglement, i.e., the Von Neumann entropy, given by

$$S(I) = -\text{Tr}[\rho_I \log(\rho_I)], \quad (21)$$

where ρ_I is the reduced state of the MPS obtained by tracing out the qubits whose indexes are in \bar{I} . Similarly, we can also compute the second Rényi entropy

$$S_2(I) = -\frac{1}{2} \log(\text{Tr}[\rho_I^2]). \quad (22)$$

Notice that the computational cost of computing S_2 scales as χ^5 , implying that we need χ to be small for this calculation to be efficient. For instance, we can see from Fig. 6 that we can readily compute S_2 for the HEA circuit, whereas the same does not apply to the QCNN.

In what follows we will define several sets of indexes leading to reduced states of interest. First, we define the simplest set $Q_j = \{j\}$, containing only index j , so that ρ_{Q_j} is the reduced density matrix on the j -th qubit, and $S(Q_j)$ quantifies the entanglement between the j -th qubit and the rest. Next, we define the set of “edge” qubits indexes $E_j = \{1, 2, \dots, j\}$, so that ρ_{E_j} is the reduced state on all the qubits from 1 to j . Finally, we define as $M_j = \{n/2 - j, n/2 - j + 1, \dots, n/2 + j\}$ as the set of “middle” qubit indexes, spanning those that spread from the middle qubit outwards with radius j .

In Figure 8 we present results for a numerical study of the entanglement properties of (the normalized) $\hat{\tau}^{(2)}|\mathcal{O}^{\otimes t}\rangle$ for the P -nets of a QCNN (top) and HEA (bottom). For the QCNN panel the system size is set to $n = 256$, thus forcing the number of layers to be $n_L = 8$, and the measurement operator is chosen to be $O = Z_1$. We show the heatmap of $S(E_j)$ for cuts at each possible index j and increasing number of layers. The inset shows an analogous plot for $S(Q_j)$. In the HEA panel we use $n = 200$ and a total number of layers $n_L = n = 200$, while the measurement operator is $O = Z_{n/2}$. This time the main plot shows

$S(Q_j)$, where we color-coded the increasing number of layers. The two insets at the left and right depict, respectively, the heatmap of $S(E_j)$ and a color-coded plot of $S_2(M_j)$. Notice that the right inset shares the same color-coding of n_L with the main plot.

As we can see from both panels in Figure 8, all the correlations are initially stored in the causal cone of O , to then quickly get washed out and become localized to the first few sites (QCNN) or completely vanish (HEA). In the QCNN case, we can particularly appreciate the switching of correlations in each of the layers' support and their later decay. For the HEA, the fact that the correlations disappear with depth can be easily interpreted by recalling that, as discussed in the previous sections, a deep HEA forms a 2-design over $U(2^n)$. One can then use Weingarten calculus to find the MPS to which $\hat{\tau}^{(2)}|O^{\otimes t}\rangle\rangle$ converges to, and prove that it corresponds to a quantum state whose distance from a product state is exponentially small in n . Namely, as shown in the appendix, we can find that for a deep HEA which forms a 2-design over $U(2^n)$, one has that $\forall j$

$$\rho_{Q_j} = \frac{1}{4^n - 1} \begin{pmatrix} 4^{n-1} - 1 & \sqrt{3}(4^{n-1} - 1) \\ \sqrt{3}(4^{n-1} - 1) & 3 \cdot 4^{n-1} \end{pmatrix}, \quad (23)$$

whose associated eigenvalues are

$$\left\{ \frac{1}{2} \left(\frac{\sqrt{-5 \cdot 4^n + 16^n + 13}}{4^n - 1} + 1 \right), \frac{1}{2} - \frac{\sqrt{-5 \cdot 4^n + 16^n + 13}}{2(4^n - 1)} \right\}$$

which leads to $S(Q_j) = 0$, as the eigenvalues converge to $\{1, 0\}$, in the $n \rightarrow \infty$ limit.

B. Local gates sampled from $G = O(4)$

In this section we will use our TN machinery to study the second moments of the expectation value for the case when U is a quantum circuit composed of two-qubit random gates ($d = 2$ and $k = 2$) drawn i.i.d. from the fundamental representation of $O(4)$. Following the same line of thought as that used to determine the P -gates for the $U(4)$ examples above, we need to find a local basis for the P -net. As indicated by Theorem 1, the local dimension of each P -gate legs is 3. In particular, we can use the following orthogonal local basis $\{|\mathbb{1}\rangle\rangle, |\mathbb{S}\rangle\rangle, |\mathbb{B}\rangle\rangle\}$, where $|\mathbb{1}\rangle\rangle, |\mathbb{S}\rangle\rangle$ are the same operators appearing in the $U(4)$ basis and where $|\mathbb{B}\rangle\rangle = |\mathbb{X} \otimes X - Y \otimes Y + Z \otimes Z\rangle\rangle$. This choice leads

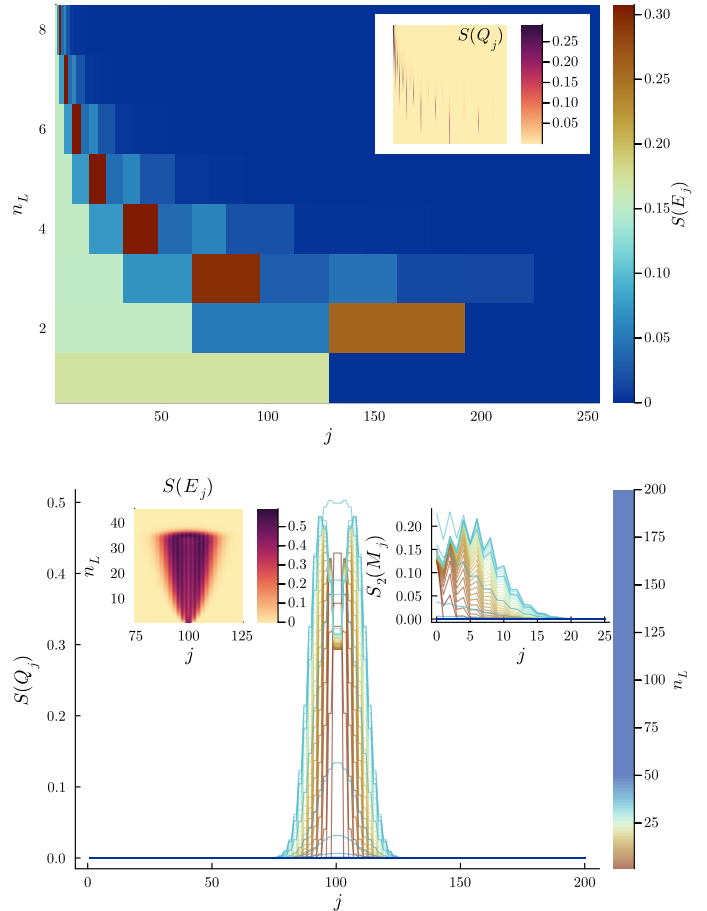


Figure 8. Entropic measures of entanglement for the vectorized MPS representation of the vectorized measurements it propagates through the P -net associated to a QCNN (top) and a HEA (bottom). Here, S and S_2 are the Von Neumann and second Rényi entropies, respectively. The entropies of Q_j quantify the entanglement between qubit j and the rest, while E_j (M_j) the one between the edge (middle) qubits and the rest (see the main text).

to 9×9 ($3 \times 3 \times 3 \times 3$ tensor) P -gates reading

$$P = \begin{pmatrix} 1 & 0 & 0 & 0 & 0 & 0 & 0 & 0 & 0 \\ 0 & 7/36 & 1/36 & 7/36 & 11/18 & 1/6 & 1/36 & 1/6 & -1/18 \\ 0 & 1/36 & 7/36 & 1/36 & -1/18 & 1/6 & 7/36 & 1/6 & 11/18 \\ 0 & 7/36 & 1/36 & 7/36 & 11/18 & 1/6 & 1/36 & 1/6 & -1/18 \\ 0 & 7/36 & 1/36 & 7/36 & 11/18 & 1/6 & 1/36 & 1/6 & -1/18 \\ 0 & 0 & 0 & 0 & 0 & 0 & 0 & 0 & 0 \\ 0 & 1/36 & 7/36 & 1/36 & -1/18 & 1/6 & 7/36 & 1/6 & 11/18 \\ 0 & 0 & 0 & 0 & 0 & 0 & 0 & 0 & 0 \\ 0 & 1/36 & 7/36 & 1/36 & -1/18 & 1/6 & 7/6 & 1/6 & 11/18 \end{pmatrix}.$$

More details on the derivation of the $O(4)$ P -gates can be found in the appendices.

Importantly, we can see from Eq. (24) that the P -matrix contains both positive and negative signs. This will lead to a Markov chain-like process matrix with non-negligible negative entries, indicating that a Monte Carlo simulation is not available. Thus, all the results presented in this section, which are obtained via our TN methods, cannot be readily reproduced via Monte Carlo sampling techniques.

We note that instead of presenting plots for the k -purities in random quantum circuits with orthogonal gates (such as those presented in the previous section), we instead opt for the more interesting route of using our TN methods to study the anticoncentration phenomenon on these circuits.

1. Anticoncentration of shallow orthogonal local random quantum circuits

Anticoncentration [4, 53] captures how much the probabilities of obtaining different outcomes when measuring a quantum circuit are similar to each other, i.e., how much the outcome probability distribution of the quantum circuit resembles that of a uniform distribution. Particularly, a random circuit architecture is said to be anticoncentrated if the probability of any measurement outcome is, at most, a constant factor larger than the uniform value. Quantitatively, anticoncentration can be studied by computing the so-called collision probability averaged over the randomly chosen circuits [4]

$$Z = \mathbb{E}_U \left[\sum_{x \in [q]^n} p_U(x)^2 \right], \quad (24)$$

where x is a computational basis state of the n -qudits circuit U , and $p_U(x)$ is the probability of measuring it as outcome. If the circuit anticoncentrates, each of the sum terms has to be at most a constant factor greater than the uniform probability q^{-n} . Hence one obtains the anticoncentration bound as the condition of the existence of a factor α independent of n such that $Z < \alpha q^{-n}$. For instance, it has been analytically shown that the outcome probabilities of one-dimensional HEAs, such as those depicted in Fig. 3(b), with local random $U(4)$ gates anticoncentrate at $n_L = \Theta(\log(n))$ depth [4]. We here analyze if a similar phenomenon will occur if the HEA gates are sampled from $O(4)$ rather than $U(4)$.

First, let us note that given a circuit U with local Haar random $O(4)$ gates, all the computational basis states will be equiprobable (as long as at least one gate acts on each qubit). This follows from the fact that the bit-flip transformation X is in $SO(4)$. Hence, we can study

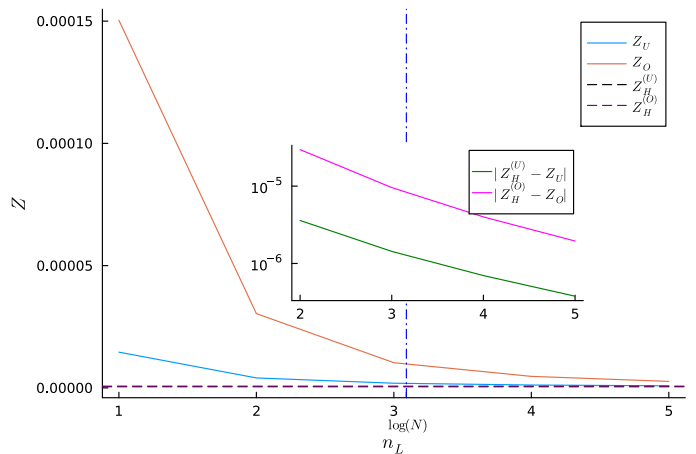


Figure 9. Averaged collision probability $Z_{U/O}$ for a one-dimensional HEA composed of local random gates sampled i.i.d. from $O(4)$ (orange line) and $U(4)$ (blue line) and acting on $n = 22$ qubits, as a function of the number of layers n_L . The dashed lines show $Z_H^{(U/O)}$, the asymptotic value of $Z_{U/O}$ as n_L tends to infinity. The inset shows the behavior in a neighborhood of $n_L = \log(n)$.

the anticoncentration by analyzing the simplified quantity $Z = q^n \mathbb{E}_U [p_U(|0\rangle^n)^2]$. Moreover, we can readily obtain the value Z_H at which Z will converge in the limit of infinite depth, i.e., when U becomes a random sample from the global $O(2^n)$, which reads $Z_H = 3/(2^n + 2)$ [24].

In Figure 9 we show the behavior of Z as a function of the number of layers n_L for a circuit acting on $n = 22$ qubits. For comparison, we also show the same behavior for the HEA with local gates samples from $U(4)$ (i.e., the case analyzed in [4]). Here, we can see that as the number of layers increases, the average collision probability quickly converge to their infinite depth limit. We can clearly see that for all values of n_L the value of Z is smaller for a circuit with unitary random gates (which is expected due to its larger expressive power). Nonetheless, it seems like random quantum circuits with orthogonal gates still anticoncentrate at logarithmic depth.

VII. DISCUSSION

Tensor networks have emerged as a crucial tool in the realm of statistical physics and condensed matter physics. The significance of tensor networks lies in their ability to represent complex correlations efficiently, allowing for the exploration of evolutions in vector spaces that are otherwise computationally intractable. Importantly, unlike

Monte Carlo techniques, which struggle with process matrices exhibiting a negative sign, tensor networks offer an alternative approach that sidesteps this issue.

In this work, we follow suit in this line of thought and ask the question: “*Can we use tensor networks, instead of Monte Carlo sampling, to exactly compute the moments of expectation values obtained from quantum circuits composed of local random gates?*” Our question is motivated from the fact that the moments can be expressed –via vectorization– as the inner product between two vectors and a Markov chain-like process matrix. Indeed, we not only show that this approach is mathematically sound, but also advantageous over standard Monte Carlo sampling techniques.

Our first main contribution is a description of the mathematical framework needed to exactly compute quantities such as $\mathbb{E}_U[\text{Tr}[U\rho U^\dagger O]^t]$ via tensor networks. The formalism is presented in a general way, allowing for local gates acting on different number of qubits, and being uniformly sampled from different local groups. We then use representation theoretical tools to derive theoretical results which analyze the local dimension of the tensor, as well as present bounds for the maximum bond dimension of the matrix product states that deep circuits can produce. Next, we showcase our method for estimating the second moment of two-types of quantum neural networks with local two-qubit gates sampled from the fundamental representations of $U(4)$ and $O(4)$. Here, we illustrate that our methods can efficiently tackle circuits acting on thousands of qubits, and composed of thousands of gates. These results also illustrate the fact that tensor networks can significantly outperform Monte Carlo simulations in terms of the desired estimation accuracy, but also by being able to tackle tasks where Monte Carlo would exhibit sign problems (local orthogonal circuit anticoncentration), or not be appropriate (computing entropic properties of the MPS).

While our numerical simulations have demonstrated the capabilities of the use of TN to study random quantum circuits, there are also many open questions and new research directions opened by our results. For instance, we naturally expect that our proposed techniques will encounter issues for problems with complicate topologies, or when the local tensor dimensions leads to prohibitively large bond dimensions. In this context, we note that it is not clear to us how to derive general bounds for the local tensor dimensions, and we expect that a rigorous mathematical analysis will be needed on a case-by-case basis (see for instance our

results in Theorem 2 for free-fermion circuits with gates sampled from $SO(4) \simeq SU(2) \oplus SU(2)$). We leave for future work a detail exploration of this optimal local basis questions, and we hope that representation theoretic tools can be used to make progress in this regard. Then, we also note that the representation of the circuit moment operator itself could be used to learn properties of the quantum circuit independently of the initial state and measurement operator. For instance, we could use density matrix renormalization group techniques to obtain its eigenvalues, and thus be able to predict the number of layers needed for the circuit to become a t -design over G_U . On a similar note, it is worth highlighting that having access to a matrix product state representation of $\hat{\tau}^{(t)}|\rho^{\otimes t}\rangle\rangle$ allows a whole new dimension of random quantum circuit analysis, such as the study of the entanglement and entropic properties of this quantum state. We leave for future work a more detailed analysis of what additional insights such analysis can provide us. Finally, we note that the proposed tensor network formalism can be readily applied to random quantum circuits with intermediate measurements, thus enabling the study of monitored random dynamics and measurement-induced criticality [54–57]. As such, given the versatility of our proposed techniques, we envision that tensor networks will quickly become a standard tool in the toolbox of quantum information scientist studying and working with circuits composed of random local gates.

Note added: A few days before our manuscript was uploaded as a preprint, we became aware of the work [58], which presents a method for treating the P -net as a TN similar to one presented here. We note that while some of the techniques in Ref. [58] are similar to ours, that work only considered the case of local unitary gates. As such, the extension to local orthogonal or free-fermionic gates gates introduced here is, to our knowledge, completely novel.

VIII. ACKNOWLEDGMENTS

We sincerely thank Hsin-Yuan (Robert) Huang, Martin Larocca, Diego García-Martín, and Francesco Caravelli for useful discussions. The authors were supported by the Laboratory Directed Research and Development (LDRD) program of Los Alamos National Laboratory (LANL) under project numbers 20230049DR (P.Braccia and L.C), and 20230527ECR (P.Bermejo and M.C.). P. Bermejo acknowledges DIPC for constant support. M.C. was also initially supported by LANL ASC Beyond Moore’s Law project.

-
- [1] S. Boixo, S. V. Isakov, V. N. Smelyanskiy, R. Babbush, N. Ding, Z. Jiang, M. J. Bremner, J. M. Martinis, and H. Neven, Characterizing quantum supremacy in near-term devices, *Nature Physics* **14**, 595 (2018).
- [2] F. Arute, K. Arya, R. Babbush, D. Bacon, J. C. Bardin, R. Barends, R. Biswas, S. Boixo, F. G. S. L. Brandao, D. A. Buell, B. Burkett, Y. Chen, Z. Chen, B. Chiaro, R. Collins, W. Courtney, A. Dunsworth, E. Farhi, B. Foxen, A. Fowler, C. Gidney, M. Giustina, R. Graff, K. Guerin, S. Habegger, M. P. Harrigan, M. J. Hartmann, A. Ho, M. Hoffmann, T. Huang, T. S. Humble, S. V. Isakov, E. Jeffrey, Z. Jiang, D. Kafri, K. Kechedzhi, J. Kelly, P. V. Klimov, S. Knysh, A. Korotkov, F. Kostritsa, D. Landhuis, M. Lindmark, E. Lucero, D. Lyakh, S. Mandrà, J. R. McClean, M. McEwen, A. Megrant, X. Mi, K. Michielsen, M. Mohseni, J. Mutus, O. Naaman, M. Neeley, C. Neill, M. Y. Niu, E. Ostby, A. Petukhov, J. C. Platt, C. Quintana, E. G. Rieffel, P. Roushan, N. C. Rubin, D. Sank, K. J. Satzinger, V. Smelyanskiy, K. J. Sung, M. D. Trevithick, A. Vainsencher, B. Villalonga, T. White, Z. J. Yao, P. Yeh, A. Zalcman, H. Neven, and J. M. Martinis, Quantum supremacy using a programmable superconducting processor, *Nature* **574**, 505 (2019).
- [3] Y. Wu, W.-S. Bao, S. Cao, F. Chen, M.-C. Chen, X. Chen, T.-H. Chung, H. Deng, Y. Du, D. Fan, *et al.*, Strong quantum computational advantage using a superconducting quantum processor, *Physical Review Letters* **127**, 180501 (2021).
- [4] A. M. Dalzell, N. Hunter-Jones, and F. G. S. L. Brandão, Random quantum circuits anticentralize in log depth, *PRX Quantum* **3**, 010333 (2022).
- [5] M. Oszmaniec, N. Dangniam, M. E. Morales, and Z. Zimborás, Fermion sampling: a robust quantum computational advantage scheme using fermionic linear optics and magic input states, *PRX Quantum* **3**, 020328 (2022).
- [6] H.-Y. Huang, R. Kueng, G. Torlai, V. V. Albert, and J. Preskill, Provably efficient machine learning for quantum many-body problems, *Science* **377**, eabk3333 (2022).
- [7] A. Nahum, J. Ruhman, S. Vijay, and J. Haah, Quantum entanglement growth under random unitary dynamics, *Physical Review X* **7**, 031016 (2017).
- [8] C. W. von Keyserlingk, T. Rakovszky, F. Pollmann, and S. L. Sondhi, Operator hydrodynamics, otocs, and entanglement growth in systems without conservation laws, *Physical Review X* **8**, 021013 (2018).
- [9] A. Nahum, S. Vijay, and J. Haah, Operator spreading in random unitary circuits, *Physical Review X* **8**, 021014 (2018).
- [10] J. R. McClean, S. Boixo, V. N. Smelyanskiy, R. Babbush, and H. Neven, Barren plateaus in quantum neural network training landscapes, *Nature Communications* **9**, 1 (2018).
- [11] M. Cerezo, A. Sone, T. Volkoff, L. Cincio, and P. J. Coles, Cost function dependent barren plateaus in shallow parametrized quantum circuits, *Nature Communications* **12**, 1 (2021).
- [12] A. Pesah, M. Cerezo, S. Wang, T. Volkoff, A. T. Sornborger, and P. J. Coles, Absence of barren plateaus in quantum convolutional neural networks, *Physical Review X* **11**, 041011 (2021).
- [13] J. Napp, Quantifying the barren plateau phenomenon for a model of unstructured variational ansätze, *arXiv preprint arXiv:2203.06174* (2022).
- [14] M. Ragone, B. N. Bakalov, F. Sauvage, A. F. Kemper, C. O. Marrero, M. Larocca, and M. Cerezo, A unified theory of barren plateaus for deep parametrized quantum circuits, *arXiv preprint arXiv:2309.09342* (2023).
- [15] E. Fontana, D. Herman, S. Chakrabarti, N. Kumar, R. Yalovetzky, J. Heredge, S. Hari Sureshbabu, and M. Pistoia, The adjoint is all you need: Characterizing barren plateaus in quantum ansätze, *arXiv preprint arXiv:2309.07902* (2023).
- [16] N. L. Diaz, D. García-Martín, S. Kazi, M. Larocca, and M. Cerezo, Showcasing a barren plateau theory beyond the dynamical lie algebra, *arXiv preprint arXiv:2310.11505* (2023).
- [17] A. Letcher, S. Woerner, and C. Zoufal, From tight gradient bounds for parameterized quantum circuits to the absence of barren plateaus in qgans, *arXiv preprint arXiv:2309.12681* (2023).
- [18] S. Thanaslip, S. Wang, N. A. Nghiem, P. J. Coles, and M. Cerezo, Subtleties in the trainability of quantum machine learning models, *Quantum Machine Intelligence* **5**, 21 (2023).
- [19] E. R. Anschuetz and B. T. Kiani, Quantum variational algorithms are swamped with traps, *Nature Communications* **13**, 7760 (2022).
- [20] E. R. Anschuetz, Critical points in quantum generative models, *International Conference on Learning Representations* (2022).
- [21] L. Monbroussou, J. Landman, A. B. Grilo, R. Kukla, and E. Kashefi, Trainability and expressivity of hamming-weight preserving quantum circuits for machine learning, *arXiv preprint arXiv:2309.15547* (2023).
- [22] A. A. Mele, Introduction to haar measure tools in quantum information: A beginner's tutorial, *arXiv preprint arXiv:2307.08956* (2023).
- [23] M. Ragone, Q. T. Nguyen, L. Schatzki, P. Braccia, M. Larocca, F. Sauvage, P. J. Coles, and M. Cerezo, Representation theory for geometric quantum machine learning, *arXiv preprint arXiv:2210.07980* (2022).
- [24] D. García-Martín, M. Larocca, and M. Cerezo, Deep quantum neural networks form gaussian processes, *arXiv preprint arXiv:2305.09957* (2023).
- [25] P. Hayden and J. Preskill, Black holes as mirrors: quantum information in random subsystems, *Journal of High Energy Physics* **9**, 120 (2007).
- [26] Y. Sekino and L. Susskind, Fast scramblers, *Journal of High Energy Physics* **2008**, 065 (2008).

- [27] W. Brown and O. Fawzi, Scrambling speed of random quantum circuits, [arXiv preprint arXiv:1210.6644](#) (2012).
- [28] N. Lashkari, D. Stanford, M. Hastings, T. Osborne, and P. Hayden, Towards the fast scrambling conjecture, *Journal of High Energy Physics* **2013**, 1 (2013).
- [29] P. Hosur, X.-L. Qi, D. A. Roberts, and B. Yoshida, Chaos in quantum channels, *Journal of High Energy Physics* **2016**, 1 (2016).
- [30] N. Hunter-Jones, Unitary designs from statistical mechanics in random quantum circuits, [arXiv preprint arXiv:1905.12053](#) (2019).
- [31] B. Barak, C.-N. Chou, and X. Gao, Spoofing linear cross-entropy benchmarking in shallow quantum circuits, [arXiv preprint arXiv:2005.02421](#) (2020).
- [32] A. Harrow and S. Mehraban, Approximate unitary t -designs by short random quantum circuits using nearest-neighbor and long-range gates, [arXiv preprint arXiv:1809.06957](#) (2018).
- [33] P. Hayden, S. Nezami, X.-L. Qi, N. Thomas, M. Walter, and Z. Yang, Holographic duality from random tensor networks, *Journal of High Energy Physics* **2016**, 1 (2016).
- [34] G. Pan and Z. Y. Meng, Sign problem in quantum monte carlo simulation, in *Encyclopedia of Condensed Matter Physics (Second Edition)* (Academic Press, 2024) second edition ed., pp. 879–893.
- [35] X. Mi, P. Roushan, C. Quintana, S. Mandra, J. Marshall, C. Neill, F. Arute, K. Arya, J. Atalaya, R. Babbush, *et al.*, Information scrambling in quantum circuits, *Science* **374**, 1479 (2021).
- [36] R. Orús, A practical introduction to tensor networks: Matrix product states and projected entangled pair states, *Annals of Physics* **349**, 117 (2014).
- [37] J. Biamonte and V. Bergholm, Tensor networks in a nutshell, [arXiv preprint arXiv:1708.00006](#) (2017).
- [38] M. Larocca, F. Sauvage, F. M. Sbahi, G. Verdon, P. J. Coles, and M. Cerezo, Group-invariant quantum machine learning, *PRX Quantum* **3**, 030341 (2022).
- [39] R. Goodman and N. R. Wallach, *Symmetry, representations, and invariants*, Vol. 255 (Springer, 2009).
- [40] E. Kökcü, D. Camps, L. B. Oftung, J. K. Freericks, W. A. de Jong, R. Van Beeumen, and A. F. Kemper, Algebraic compression of quantum circuits for hamiltonian evolution, *Physical Review A* **105**, 032420 (2022).
- [41] R. Wiersema, E. Kökcü, A. F. Kemper, and B. N. Bakalov, Classification of dynamical lie algebras for translation-invariant 2-local spin systems in one dimension, [arXiv preprint arXiv:2309.05690](#) (2023).
- [42] B. Pozsgay, Quantum circuits with free fermions in disguise, [arXiv preprint arXiv:2402.02984](#) (2024).
- [43] R. Zeier and T. Schulte-Herbrüggen, Symmetry principles in quantum systems theory, *Journal of mathematical physics* **52**, 113510 (2011).
- [44] M. Larocca, P. Czarnik, K. Sharma, G. Muraleedharan, P. J. Coles, and M. Cerezo, Diagnosing Barren Plateaus with Tools from Quantum Optimal Control, *Quantum* **6**, 824 (2022).
- [45] A. W. Harrow and R. A. Low, Random quantum circuits are approximate 2-designs, *Communications in Mathematical Physics* **291**, 257 (2009).
- [46] F. G. Brandao, A. W. Harrow, and M. Horodecki, Local random quantum circuits are approximate polynomial-designs, *Communications in Mathematical Physics* **346**, 397 (2016).
- [47] J. Haferkamp, Random quantum circuits are approximate unitary t -designs in depth $O\left(nt^{5+o(1)}\right)$, *Quantum* **6**, 795 (2022).
- [48] J. Haah, Y. Liu, and X. Tan, Efficient approximate unitary designs from random pauli rotations, [arXiv preprint arXiv:2402.05239](#) (2024).
- [49] C.-F. Chen, J. Docter, M. Xu, A. Bouland, and P. Hayden, Efficient unitary t -designs from random sums, [arXiv preprint arXiv:2402.09335](#) (2024).
- [50] I. Cong, S. Choi, and M. D. Lukin, Quantum convolutional neural networks, *Nature Physics* **15**, 1273 (2019).
- [51] A. Kandala, A. Mezzacapo, K. Temme, M. Takita, M. Brink, J. M. Chow, and J. M. Gambetta, Hardware-efficient variational quantum eigensolver for small molecules and quantum magnets, *Nature* **549**, 242 (2017).
- [52] L. Leone, S. F. Oliviero, L. Cincio, and M. Cerezo, On the practical usefulness of the hardware efficient ansatz, [arXiv preprint arXiv:2211.01477](#) (2022).
- [53] D. Hangleiter, J. Bermejo-Vega, M. Schwarz, and J. Eisert, Anticoncentration theorems for schemes showing a quantum speedup, *Quantum* **2**, 65 (2018).
- [54] C.-M. Jian, Y.-Z. You, R. Vasseur, and A. W. Ludwig, Measurement-induced criticality in random quantum circuits, *Physical Review B* **101**, 104302 (2020).
- [55] Y. Bao, S. Choi, and E. Altman, Theory of the phase transition in random unitary circuits with measurements, *Physical Review B* **101**, 104301 (2020).
- [56] A. Nahum, S. Roy, B. Skinner, and J. Ruhman, Measurement and entanglement phase transitions in all-to-all quantum circuits, on quantum trees, and in landau-ginsburg theory, *PRX Quantum* **2**, 010352 (2021).
- [57] M. P. Fisher, V. Khemani, A. Nahum, and S. Vijay, Random quantum circuits, *Annual Review of Condensed Matter Physics* **14**, 335 (2023).
- [58] H.-Y. Hu, A. Gu, S. Majumder, H. Ren, Y. Zhang, D. S. Wang, Y.-Z. You, Z. Mineev, S. F. Yelin, and A. Seif, Demonstration of robust and efficient quantum property learning with shallow shadows, [arXiv preprint arXiv:2402.17911](#) (2024).
- [59] Z. Zimborás, R. Zeier, M. Keyl, and T. Schulte-Herbrüggen, A dynamic systems approach to fermions and their relation to spins, *EPJ Quantum Technology* **1**, 1 (2014).
- [60] E. Kökcü, T. Steckmann, Y. Wang, J. Freericks, E. F. Dumitrescu, and A. F. Kemper, Fixed depth hamiltonian simulation via cartan decomposition, *Physical Review Letters* **129**, 070501 (2022).
- [61] R. Jozsa and A. Miyake, Matchgates and classical simulation of quantum circuits, *Proceedings of the Royal Society*

Appendix A: Proof of Theorem 1 and Proposition 1

In what follows, we present a joint proof for Theorem 1 and Proposition 1. For simplicity we start by considering the case when all the local gates are sampled from $G = U(d^k)$, and the study the case of $G = O(d^k), SP(d^k/n)$.

Proof. Let V be a unitary acting on k -qudits. Then, we know from the Schur-Weyl duality that the t -th order commutant of the fundamental representation of the unitary group $U(d^k)$ is spanned by the subsystem permuting representation of the symmetric group S_t . Specifically, the subsystem permuting representation of a permutation $\sigma \in S_t$ is

$$P(\sigma) = \sum_{i_1, \dots, i_k=1}^{d^k} |i_{\sigma^{-1}(1)}, \dots, i_{\sigma^{-1}(k)}\rangle \langle i_1, \dots, i_k|, \quad (\text{A1})$$

from which it can be verified that $[V^{\otimes t}, P(\sigma)] = 0$ for any $V \in U(d^k)$ and for all $\sigma \in S_t$.

Next, let us note that any permutation of the t -copies of the k -qudit Hilbert space can be expressed as

$$P(\sigma) = \bigotimes_{\mu=1}^k P_{\mu}(\sigma), \quad (\text{A2})$$

where $P_{\mu}(\sigma)$ permutes the copies of the μ -th qudits. From this, it follows that in the vectorized formalism we can express

$$|P(\sigma)\rangle\rangle = \bigotimes_{\mu=1}^k |P_{\mu}(\sigma)\rangle\rangle, \quad (\text{A3})$$

indicating that $|P(\sigma)\rangle\rangle$ is an MPS of bond dimension one. Thus, since there are $t!$ operators in S_t , and since each one of them corresponds to a bond dimension one MPS, we can always construct the P matrix for the moment operator in a tensor product basis where each $P(\sigma)$ is a basis element, leading to P being a square matrix of dimension up to $(t!)^2 \times (t!)^2$.

From here, it is not hard to see that if the group is $G_U = U(d^n)$, then since $\hat{\tau}^{(t)}$ will be a projector onto $\text{comm}^{(t)}(U(d^n))$, then for any $A \in \mathcal{B}(\mathcal{H}^{\otimes t})$, the vectorized operator $\hat{\tau}^{(t)}|A\rangle\rangle$ will be a linear combination of the $|P(\sigma)\rangle\rangle$. Since there are $t!$ of them, and since they are all bond dimension-one MPSs, the maximum bond dimension of the vector $\hat{\tau}^{(t)}|A\rangle\rangle$ is $t!$.

Next, let us consider the case of $O(d^k)$ and $Sp(d^k/2)$ (assuming d is even). Here, we know from the Schur-Weyl duality that the t -th order commutant of the fundamental representation of the orthogonal group $O(d^k)$ is spanned

by the Brauer algebra B_{2t} [38]. Given that the t -th order commutant of $Sp(d^k/2)$ follows the same structure as the Brauer algebra, we will focus on the orthogonal group, with the proof of the symplectic group following similarly.

Here, we only need to know that for any element σ of the Brauer algebra it follows that

$$|P(\sigma)\rangle\rangle = \bigotimes_{\mu=1}^k |P_\mu(\sigma)\rangle\rangle, \quad (\text{A4})$$

meaning that the P matrices can also always be constructed in a basis where each $|P(\sigma)\rangle\rangle$ is a basis element. Hence, since there are $\frac{(2t!)}{2^{t!}}$ such elements, the P matrix will be square and of dimension up to $\left(\frac{(2t!)}{2^{t!}}\right)^2 \times \left(\frac{(2t!)}{2^{t!}}\right)^2$. With a similar reasoning, the maximum bond dimension of any operator projected by the t -th moment operator of a deep circuit with $G_U = O(d^n)$ will be $\frac{(2t!)}{2^{t!}}$. \square

Appendix B: Proof of Theorem 2 and Proposition 2

In this section we present a proof for Theorem 2 and Proposition 2 an n -qubit circuit composed of free-fermionic gates [16]. First, let us recall a few basic properties of the free-fermionic representation of the group $SO(2n)$. To begin, we recall that the Lie algebra $\mathfrak{so}(2n)$ associated to this group has a basis given by [41, 59, 60]

$$\mathfrak{so}(2n) = \text{span}_{\mathbb{R}} i\{\widehat{Z_i}, \widehat{X_i X_j}, \widehat{Y_i Y_j}, \widehat{X_i Y_j}, \widehat{Y_i X_j}\}_{1 \leq i < j \leq n}, \quad (\text{B1})$$

where we use the notation $\widehat{A_i B_j} = A_i Z_i Z_{i+1} \cdots Z_{j-1} B_j$. To work with this algebra, it is convenient to define the $2n$ Majorana operators [61]

$$\begin{aligned} c_1 &= X \mathbb{1} \dots \mathbb{1}, \quad c_3 = ZX \mathbb{1} \dots \mathbb{1}, \dots, \quad c_{2n-1} = Z \dots ZX \\ c_2 &= Y \mathbb{1} \dots \mathbb{1}, \quad c_4 = ZY \mathbb{1} \dots \mathbb{1}, \dots, \quad c_{2n} = Z \dots ZY, \end{aligned}$$

which are proportional to Pauli operators that satisfy the anti-commutation relation

$$\{c_\mu, c_\nu\} = 2\delta_{\mu\nu} \quad \mu, \nu = 1, \dots, 2n. \quad (\text{B2})$$

In this basis, all the elements of $\mathfrak{so}(2n)$ in (B1) can be expressed as the product of two Majoranas. That is,

$$\mathfrak{so}(2n) = \text{span}_{\mathbb{R}} \{c_\mu c_\nu\}_{1 \leq \mu < \nu \leq 2n}. \quad (\text{B3})$$

Next, we note that the adjoint action of $SO(2n)$ over the operator space $\mathcal{B}(\mathcal{H})$ is in itself a representation of the

Lie group, and hence induced a decomposition of $\mathcal{B}(\mathcal{H})$ into invariant subspaces, or group-modules. In particular, one can prove that $\mathcal{B}(\mathcal{H})$ can be decomposed into modules as [16]

$$\mathcal{B}(\mathcal{H}) = \bigoplus_{\kappa=0}^{2n} \mathcal{B}_\kappa, \quad (\text{B4})$$

where each \mathcal{B}_κ is the linear space, of dimension $\binom{2n}{\kappa}$, spanned by a basis of products of κ distinct Majoranas. As such, we know that given any $A \in \mathcal{B}_\kappa$, then $VAV^\dagger \in \mathcal{B}_\kappa$ for any $V \in SO(2n)$.

Having characterized the Lie group and its associated Lie algebra, let us proceed to study their t -th fold commutants. First, for $t = 1$, we know that the only symmetry of the group is the fermionic parity operator $X^{\otimes n} = (-i)^n c_1 c_2 \cdots c_{2n}$, so that

$$\text{comm}^{(1)}(SO(2n)) = \text{span}_{\mathbb{C}} \{\mathbb{1}, X^{\otimes n}\}. \quad (\text{B5})$$

Then, an orthonormal basis of size $2(2n + 1)$ for $\text{comm}^{(2)}(SO(2n))$ is given by [5, 16]

$$\begin{aligned} Q_\kappa^0 &= \mathcal{N}_\kappa \sum_{\mathbf{s} \in \binom{[2n]}{\kappa}} c^{\mathbf{s}} \otimes c^{\mathbf{s}}, \\ Q_\kappa^1 &= \mathcal{N}_\kappa (-i)^n i^{\kappa \bmod 2} \sum_{\mathbf{s} \in \binom{[2n]}{\kappa}} (-1)^{\pi(\mathbf{s})} c^{\mathbf{s}} \otimes c^{\bar{\mathbf{s}}}, \end{aligned} \quad (\text{B6})$$

for integers $0 \leq \kappa \leq 2n$, and $\mathcal{N}_\kappa = \left(2^n \sqrt{\binom{2n}{\kappa}}\right)^{-1}$.

With these results in mind, let us first prove Theorem 2.

Proof. Let V be a two-qubit gate sampled from the Haar measure of the free-fermionic representation of the group $SO(4)$. Then, according to Eq. (B6), a basis for $\text{comm}^{(2)}(SO(2n))$ contains 10 elements. For simplicity, let us first consider the first five parity respecting elements Q_κ^0 which we can express in the Pauli basis as

$$\begin{aligned} Q_0^0 &= \mathbb{1} \mathbb{1} \otimes \mathbb{1} \mathbb{1} \\ Q_1^0 &= X \mathbb{1} \otimes X \mathbb{1} + Y \mathbb{1} \otimes Y \mathbb{1} + ZX \otimes ZX + ZY \otimes ZY \\ Q_2^0 &= Z \mathbb{1} \otimes Z \mathbb{1} + \mathbb{1} Z \otimes \mathbb{1} Z + XX \otimes XX + XY \otimes XY \\ &\quad + YY \otimes YY + YX \otimes YX \\ Q_3^0 &= \mathbb{1} X \otimes \mathbb{1} X + \mathbb{1} Y \otimes \mathbb{1} Y + XZ \otimes XZ + YZ \otimes YZ \\ Q_4^0 &= ZZ \otimes ZZ \end{aligned}$$

Here, a Pauli operator $AB \otimes CD$ is read as: A and B act on the first and second qubits, respectively, of the first copy of the Hilbert space; while C and D act on the first and second qubits, respectively, of the second copy of the Hilbert space.

By vectorizing this operator, and re-ordering the indexes of the tensor product to $AB \otimes CD \rightarrow |AC\rangle\rangle \otimes |BD\rangle\rangle$, and omitting redundancies as $|A\rangle\rangle|B\rangle\rangle \equiv |AA\rangle\rangle \otimes |BB\rangle\rangle$ we find

$$\begin{aligned} |Q_0^0\rangle\rangle &= |\mathbb{1}\rangle\rangle|\mathbb{1}\rangle\rangle \\ |Q_1^0\rangle\rangle &= |X+Y\rangle\rangle|\mathbb{1}\rangle\rangle + |Z\rangle\rangle|X+Y\rangle\rangle \\ |Q_2^0\rangle\rangle &= |Z\rangle\rangle|\mathbb{1}\rangle\rangle + |\mathbb{1}\rangle\rangle|Z\rangle\rangle + |X+Y\rangle\rangle|X+Y\rangle\rangle \\ |Q_3^0\rangle\rangle &= |\mathbb{1}\rangle\rangle|X+Y\rangle\rangle + |X+Y\rangle\rangle|Z\rangle\rangle \\ |Q_4^0\rangle\rangle &= |Z\rangle\rangle|Z\rangle\rangle \end{aligned}$$

which shows that the local commutant's basis for the vectorized (parity respecting) 2-nd order commutant of $SO(4n)$ is composed of three elements $\{|\mathbb{1}\rangle\rangle, |Z\rangle\rangle, |X+Y\rangle\rangle\}$. A similar procedure can be performed on the rest of the elements Q_κ^1 , which will lead to three additional basis vectors. Therefore, the P matrix for $\hat{\tau}_{SO(4)}^{(2)}$ will be of dimension 9×9 if either ρ or O have fixed fermionic parity (as we only need to keep the basis elements coming from the Q_κ^0 operators), while it will be of size 36×36 for generic states and observables. \square

Next, let us provide a proof for Proposition 2.

Proof. First, let us recall that we assume that the random circuit U forms a 2-design over $SO(2n)$. Then, we know that the circuit moment operator $\hat{\tau}^{(2)}$ will be a projector onto the commutant $\text{comm}^{(2)}(SO(2n))$ spanned by the $2(2n+1)$ elements in Eq. (B6). If A is a Pauli operator belonging to $\mathfrak{iso}(2n)$, then we know that $A^{\otimes 2}$ can only have non-zero overlap with the Casimir operator Q_2^0 . A direct calculation reveals that $\text{Tr}[Q_\kappa^j A^{\otimes 2}] = \delta_{j,0} \delta_{\kappa,2} \langle\langle Q_2^0 | A \rangle\rangle = \delta_{j,0} \delta_{\kappa,2} 2^n \mathcal{N}_\kappa$. More precisely, we have that $2^n \mathcal{N}_2 = 1/\sqrt{\binom{2n}{\kappa}} \in \Omega(1/\text{poly}(n))$.

From the previous, find

$$\begin{aligned} \hat{\tau}^{(2)} |A^{\otimes 2}\rangle\rangle &= \sum_{j=0,1} \sum_{\kappa=0}^{2n} |Q_\kappa^j\rangle\rangle \langle\langle Q_\kappa^j | A^{\otimes 2} \rangle\rangle \\ &= \frac{1}{\sqrt{\binom{2n}{\kappa}}} |Q_2^0\rangle\rangle. \end{aligned} \quad (\text{B7})$$

Hence, the maximum bond dimension of $\hat{\tau}^{(2)} |A^{\otimes 2}\rangle\rangle$ will be equal to that of $|Q_2^0\rangle\rangle$. Denoting as $S = \{Z_i, \widehat{X_i X_j}, \widehat{Y_i Y_j}, \widehat{X_i Y_j}, \widehat{Y_i X_j}\}$ the basis for $\mathfrak{iso}(2n)$, we know that we can express Q_2^0 as $\sum_{P \in S} P \otimes P$. A direct vectorization of this operator, along with a basis reordering and elimination of redundancies leads to

$$|Q_2^0\rangle\rangle \propto \sum_{j=1}^n |Z_j\rangle\rangle + \sum_{1 \leq i < j \leq n} |(X_i + \widehat{Y_i})(\widehat{X_j} + Y_j)\rangle\rangle, \quad (\text{B8})$$

where

$$|(X_i + \widehat{Y_i})(\widehat{X_j} + Y_j)\rangle\rangle = |(X_i + Y_i) Z_{i+1} \cdots Z_{j-1} (X_j + Y_j)\rangle\rangle.$$

From here, we need to show that this an MPS of bond dimension $\chi = 3$. For this purpose, we use the following lemma.

Lemma 1. *The state*

$$|\psi\rangle = \sum_{i=1}^n |0 \dots 0 1_i 0 \dots 0\rangle + \sum_{1 \leq i < j \leq n} |0 \dots 0 2_i 1 \dots 1 2_j 0 \dots 0\rangle$$

can be described by the following (bond dimension $\chi = 3$) MPS:

$$\begin{array}{c} L \quad A \quad \cdots \quad A \quad R \\ \bullet \quad \bullet \quad \cdots \quad \bullet \quad \bullet \\ | \quad | \quad \quad \quad | \quad | \end{array}, \quad (\text{B9})$$

where

$$\begin{aligned} \begin{array}{c} L \\ \bullet \\ | \end{array} \nu &= [|0\rangle \ |1\rangle \ |2\rangle]_\nu, \\ \mu \begin{array}{c} A \\ \bullet \\ | \end{array} \nu &= \begin{bmatrix} |0\rangle & |1\rangle & |2\rangle \\ 0 & |0\rangle & 0 \\ 0 & |2\rangle & |1\rangle \end{bmatrix}_{\mu,\nu}, \quad \mu \begin{array}{c} R \\ \bullet \\ | \end{array} = \begin{bmatrix} |1\rangle \\ |0\rangle \\ |2\rangle \end{bmatrix}_\mu \end{aligned} \quad (\text{B10})$$

The proof of this lemma is direct as we have explicitly constructed the MPS.

Using Lemma 1, we conclude our proof as $|Q_2^0\rangle\rangle$ can be mapped to the state $|\psi\rangle$ in the lemma via the relabeling $\mathbb{1} \rightarrow 0$, $Z \rightarrow 1$ and $(X+Y) \rightarrow 2$, and therefore is an MPS of bond dimension $\chi = 3$. \square

Appendix C: Efficient computation of the k -purities

Computing the k -purities $p_O^{(k)}$ of Eq. (20) requires computing sums over exponentially large spaces, as the number of n -qubits Paulis P_j with bodyness $|P_j| = k$ is $N_k = 3^k \binom{n}{k}$. Hence, obtaining these quantities by individually evaluating the Hilbert-Schmidt products with all the 4^N Paulis would lead to an exponential wall-time, making the method unpractical. However, we can directly obtain $p_O^{(k)}$ from the MPS representation of $\hat{\tau}^{(2)} |O^{\otimes 2}\rangle\rangle$ by computing its overlap with an MPS $|\phi_k\rangle\rangle$ that effectively projects onto the subspace of all Paulis with given bodyness k . Since the maximum bond dimension of $|\phi_k\rangle\rangle$, turns out to be $\lfloor n/2 \rfloor + 1$, with $\lfloor x \rfloor$ being the integer part of x , this computation is efficient.

In order to construct these projectors one first needs to understand how to extract the overlaps with the trivial $\mathbb{1}_j^{\otimes 2}$, and non-trivial $X_j^{\otimes 2}, Y_j^{\otimes 2}, Z_j^{\otimes 2}$ Paulis from the local $\text{comm}^{(2)}(G_j)$ bases on each of the physical legs $j \in [n]$ of the MPS $\widehat{\tau}^{(2)}|O^{\otimes 2}\rangle\rangle$ at the end of the P -net. To this end, we will introduce two vectors $|s_j^I\rangle\rangle, |s_j^P\rangle\rangle$ defined by the following properties

$$\begin{aligned} \langle\langle s_j^I | O^{\otimes 2} \rangle\rangle &= \frac{1}{4} \text{Tr}_j [\mathbb{1}_j^{\otimes 2} O^{\otimes 2}], \\ \langle\langle s_j^P | O^{\otimes 2} \rangle\rangle &= \frac{1}{4} \text{Tr}_j [(X_j^{\otimes 2} + Y_j^{\otimes 2} + Z_j^{\otimes 2}) O^{\otimes 2}], \end{aligned} \quad (\text{C1})$$

where Tr_j denotes the partial trace over the j -th qubit. For example, in the cases studied in Secs. VI A, where all the gates are drawn i.i.d. from $G = U(4)$, one finds, for the local basis $\{|\mathbb{1}\rangle\rangle, |S\rangle\rangle\}$ used therein, that the vectors $|s_j^I\rangle\rangle, |s_j^P\rangle\rangle$ exactly correspond to the basis elements $|s_j^I\rangle\rangle = |\mathbb{1}\rangle\rangle \forall j$ and $|s_j^P\rangle\rangle = |S\rangle\rangle \forall j$.

Once these vectors have been figured out, computing $p_O^{(k)}$ turns into a matter of computing the contractions of the MPS at the end of the P -net with all the possible $\binom{n}{k}$ ways we can distribute k $|s_j^P\rangle\rangle$ and $n - k$ $|s_j^I\rangle\rangle$ on its physical legs. That is, the projectors $|\phi_k\rangle\rangle$ that we are looking for can be written in the following form

$$|\phi_k\rangle\rangle = \sum_{c \in \Delta_k^n} \left(\bigotimes_{j \in c} |s_j^P\rangle\rangle \right) \otimes \left(\bigotimes_{j \notin c} |s_j^I\rangle\rangle \right), \quad (\text{C2})$$

where we defined Δ_k^n to be the set containing all the $\binom{n}{k}$ combinations of k indices from $[n]$. For example $\Delta_1^3 = \{(1), (2), (3)\}$, and $\Delta_2^3 = \{(1, 2), (1, 3), (2, 3)\}$. Notice that together, Eqs. (C1) and (C2) correctly lead to

$$p_O^{(k)} = \langle\langle \phi_k | \widehat{\tau}^{(2)} | O^{\otimes 2} \rangle\rangle, \quad (\text{C3})$$

as can be easily checked from the definition of k -purities in Eq. (20).

Then, the following Lemma shows how to build $|\phi_k\rangle\rangle$ as an MPS of maximum bond dimension $\chi = \lfloor n/2 \rfloor + 1$.

Lemma 2. *the vector $|\phi_k\rangle\rangle$ can be written as the following MPS:*

$$L_1 \quad L_2 \quad \dots \quad L_k \quad A_1 \quad \dots \quad A_{n-2k} \quad R_k \quad \dots \quad R_2 \quad R_1, \quad (\text{C4})$$

where

$$\begin{aligned} \mu \quad \begin{array}{c} L_m \\ \circ \\ \mu \quad \nu \end{array} &= \begin{bmatrix} |s_m^I\rangle\rangle & |s_m^P\rangle\rangle \\ & \ddots \\ & & |s_m^I\rangle\rangle & |s_m^P\rangle\rangle \end{bmatrix}_{\mu, \nu}, \\ \mu \quad \begin{array}{c} A_m \\ \circ \\ \mu \quad \nu \end{array} &= \begin{bmatrix} |s_{k+m}^I\rangle\rangle & |s_{k+m}^P\rangle\rangle \\ & \ddots \\ & & |s_{k+m}^I\rangle\rangle & |s_{k+m}^P\rangle\rangle \end{bmatrix}_{\mu, \nu}, \\ \mu \quad \begin{array}{c} R_m \\ \circ \\ \mu \quad \nu \end{array} &= \begin{bmatrix} |s_{n-m+1}^I\rangle\rangle \\ |s_{n-m+1}^P\rangle\rangle & \ddots \\ & \ddots & |s_{n-m+1}^I\rangle\rangle \\ & & & |s_{n-m+1}^P\rangle\rangle \end{bmatrix}_{\mu, \nu}, \end{aligned} \quad (\text{C5})$$

for all $1 \leq k \leq \lfloor n/2 \rfloor$. For $\lfloor n/2 \rfloor < k < n$ $|\phi_k\rangle\rangle$ can be recovered with the same construction after swapping $|s_j^I\rangle\rangle \leftrightarrow |s_j^P\rangle\rangle$ and changing $k \leftarrow n - k$.⁶ Lastly, the cases $k = 0, n$ are trivially recovered by $|\phi_0\rangle\rangle = \bigotimes_j |s_j^I\rangle\rangle$ and $|\phi_n\rangle\rangle = \bigotimes_j |s_j^P\rangle\rangle$, which can again be written in a simple MPS form with bond dimension $\chi = 1$.

The proof of this Lemma follows by direct inspection.

Appendix D: MPS for deep HEA circuits composed of $U(4)$ random gates

It is well known that deep n -qubit HEA quantum circuit made of local Haar random i.i.d $U(4)$ gates converge to 2-designs over the global $U(2^n)$ [32, 46]. Using Weingarten calculus we can thus compute the MPS obtained at the end of the P -net for these architectures. In particular, if we assume that U forms a 2-designs over $U(2^n)$, we have [22, 24]

$$\begin{aligned} \tau_U^2(O^{\otimes 2}) &= \frac{1}{d^2 - 1} \left(\text{Tr}[O^{\otimes 2}] - \frac{\text{Tr}[O^{\otimes 2} \text{SWAP}]}{d} \right) \mathbb{1} \otimes \mathbb{1} \\ &\quad + \frac{1}{d^2 - 1} \left(\text{Tr}[O^{\otimes 2} \text{SWAP}] - \frac{\text{Tr}[O^{\otimes 2}]}{d} \right) \text{SWAP}, \end{aligned} \quad (\text{D1})$$

⁶ Notice that when n is even, the MPS $|\phi_{n/2}\rangle\rangle$ has no A tensors.

with $d = 2^n$. Here

$$\begin{aligned} \mathbb{1} &= \bigotimes_{j=1}^n I_j, \\ \text{SWAP} &= \bigotimes_{j=1}^n \text{SWAP}_j = \bigotimes_{j=1}^n \frac{1}{2}(\mathbb{1}_j + S_j). \end{aligned} \quad (\text{D2})$$

Let us now assume all the Paulis to be normalized, i.e. $\text{Tr}[\mathbb{1}] = 1$. This leads to $\text{Tr}[S] = 3$, $\text{Tr}[\text{SWAP}] = 1/2$, $\text{Tr}[\text{SWAP}S] = 3/2$. In what follows, we find it convenient to write

$$\begin{aligned} |\mathbb{1}\rangle\rangle &= (1, 0) = |0\rangle, \\ |S\rangle\rangle &= (0, \sqrt{3}) = \sqrt{3}|1\rangle \\ |\text{SWAP}\rangle\rangle &= \frac{1}{2}(|\mathbb{1}\rangle\rangle + |S\rangle\rangle) = \frac{1}{2}(|0\rangle + \sqrt{3}|1\rangle), \end{aligned} \quad (\text{D3})$$

where we have performed a change of basis from $\{|\mathbb{1}\rangle\rangle, |S\rangle\rangle\}$ to $\{|0\rangle, |1\rangle\}$ as the latter is orthonormal.

Since we will eventually normalize the vectorized operators to interpret them as quantum states and compute their entropy, we can simply write

$$\tau_U^2(O^{\otimes 2}) \propto \text{SWAP} - \frac{\mathbb{1}}{d} \propto (I + S)^{\otimes n} - \mathbb{1}, \quad (\text{D4})$$

where we used the fact that Pauli operators are traceless. Vectorizing this operator we get

$$|\tau_U^2(O^{\otimes 2})\rangle\rangle \propto (|0\rangle + \sqrt{3}|1\rangle)^{\otimes n} - |0\rangle^{\otimes n}, \quad (\text{D5})$$

which once normalized, reads

$$|\tau_U^2(O^{\otimes 2})\rangle\rangle = \frac{(|0\rangle + \sqrt{3}|1\rangle)^{\otimes n} - |0\rangle^{\otimes n}}{\sqrt{d^2 - 1}}. \quad (\text{D6})$$

Notice that we switched the notation from $|\tau_U^2(O^{\otimes 2})\rangle\rangle$ to $|\tau_U^2(O^{\otimes 2})\rangle$ to indicate that the latter is a proper quantum state.

From here, we can compute the reduced density matrix of $|\tau_U^2(O^{\otimes 2})\rangle$ into any subsystem. In particular, we care for $\rho_{Q_j} = \text{Tr}_{\bar{j}}[|\tau_U^2(O^{\otimes 2})\rangle\langle\tau_U^2(O^{\otimes 2})|]$ where $\text{Tr}_{\bar{j}}$ indicates the partial trace over all qubits but the j -th one. In particular, since the state is permutation invariant, $\rho_{Q_j} = \rho_{Q_{j'}}$ for all $j, j' = 1, \dots, n$. Let us introduce the unnormalized state $|\phi\rangle = |0\rangle + \sqrt{3}|1\rangle$, and let us call $\alpha = 1/(d^2 - 1)$. We have

$$\begin{aligned} |\tau_U^2(O^{\otimes 2})\rangle\langle\tau_U^2(O^{\otimes 2})| &= \alpha[|\phi\rangle\langle\phi|_1 \otimes |\phi\rangle\langle\phi|^{\otimes n-1} \\ &\quad + |0\rangle\langle 0|_1 \otimes |0\rangle\langle 0|^{\otimes n-1} \\ &\quad - |\phi\rangle\langle 0|_1 \otimes |\phi\rangle\langle 0|^{\otimes n-1} \\ &\quad - |0\rangle\langle\phi|_1 \otimes |0\rangle\langle\phi|^{\otimes n-1}]. \end{aligned} \quad (\text{D7})$$

Since $\text{Tr}[|\phi\rangle\langle\phi|^{\otimes n-1}] = 4^{n-1}$, $\text{Tr}[|0\rangle\langle 0|^{\otimes n-1}] = \text{Tr}[|\phi\rangle\langle 0|^{\otimes n-1}] = \text{Tr}[|0\rangle\langle\phi|^{\otimes n-1}] = 1$, we can straightforwardly read off the reduced density matrix for any single qubit as

$$\rho_{Q_j} = \frac{1}{4^n - 1} \begin{pmatrix} 4^{n-1} - 1 & \sqrt{3}(4^{n-1} - 1) \\ \sqrt{3}(4^{n-1} - 1) & 3 \cdot 4^{n-1} \end{pmatrix}. \quad (\text{D8})$$

The eigenvalues $\lambda_1 > \lambda_2$ of this matrix are

$$\begin{aligned} \lambda_1 &= \frac{1}{2} \left(\frac{\sqrt{-5 \cdot 4^n + 16^n + 13}}{4^n - 1} + 1 \right), \\ \lambda_2 &= \frac{1}{2} - \frac{\sqrt{-5 \cdot 4^n + 16^n + 13}}{2(4^n - 1)}. \end{aligned} \quad (\text{D9})$$

Interestingly, $\lambda_2 \neq 0$, signaling that the ensuing MPS for deep circuits has a non-trivial entanglement structure (it is not a product state). However, these correlations become exponentially small as the system size n increases.

Appendix E: Derivation of the $O(4)$ P -gates

In the same spirit as the toy model presented in the main text for $U(4)$, we here show how to build the P -matrices of random circuits whose gates are sampled i.i.d. from the Haar measure of the fundamental representation of $O(4)$. We start by recalling that $\text{comm}^{(2)}(O(4))$ is [24]:

$$\text{comm}^{(2)}(O(4)) = \text{span}_{\mathbb{C}}\{\mathbb{1} \otimes \mathbb{1}, \text{SWAP}, \Pi\},$$

where Π is the unnormalized projector $\Pi = d|\Phi\rangle\langle\Phi|$ onto $|\Phi\rangle = \frac{1}{2}\sum_{i=0}^3 |ii\rangle$, the Bell state over two copies of \mathcal{H} , the (two-qubit) Hilbert space $\mathcal{H} = \mathcal{H}_1 \otimes \mathcal{H}_2$ over which a gate sampled from $O(4)$ acts on. We now notice that, analogously to the case of the SWAP operator, Π can be decomposed as $\Pi = \Pi_1 \otimes \Pi_2$, with Π_j acting on $\mathcal{H}_j^{\otimes 2}$, the two copies of the j -th qubit, and that

$$\Pi = \frac{1}{2}(\mathbb{1} + B),$$

with $B = X \otimes X - Y \otimes Y + Z \otimes Z$ and X, Y and Z the Pauli operators. With this in mind, we find it convenient to work with the following basis of $\text{comm}^{(2)}(O(4))$:

$$\{\mathbb{1} \otimes \mathbb{1}, S \otimes \mathbb{1} + \mathbb{1} \otimes S + S \otimes S, B \otimes \mathbb{1} + \mathbb{1} \otimes B + B \otimes B\},$$

where we recall the definition $S = X \otimes X + Y \otimes Y + Z \otimes Z$ from the main text. Let us now define the following two vectors

$$\begin{aligned} |A_S\rangle\rangle &= (|S\rangle\rangle|\mathbb{1}\rangle\rangle + |\mathbb{1}\rangle\rangle|S\rangle\rangle + |S\rangle\rangle|S\rangle\rangle), \\ |A_B\rangle\rangle &= (|B\rangle\rangle|\mathbb{1}\rangle\rangle + |\mathbb{1}\rangle\rangle|B\rangle\rangle + |B\rangle\rangle|B\rangle\rangle). \end{aligned}$$

Given these, we can express the vectorized basis of $\text{comm}^{(2)}(O(4))$ as

$$\{|\mathbb{1}\rangle|\mathbb{1}\rangle, |A_S\rangle, |A_B\rangle\}. \quad (\text{E1})$$

We can now compute the action of the second moment operator $\hat{\tau}_{O(4)}^{(2)}$ on each distinct tensor product of two elements from $\{|\mathbb{1}\rangle, |S\rangle, |B\rangle\}$. We find

$$\begin{aligned} \hat{\tau}_{SO(4)}^{(2)}|\mathbb{1}\rangle|\mathbb{1}\rangle &= |\mathbb{1}\rangle|\mathbb{1}\rangle, \\ \hat{\tau}_{SO(4)}^{(2)}|S\rangle|\mathbb{1}\rangle &= \hat{\tau}_{SO(4)}^{(2)}|\mathbb{1}\rangle|S\rangle = \frac{7}{36}A_2 + \frac{1}{36}A_3, \\ \hat{\tau}_{SO(4)}^{(2)}|S\rangle|B\rangle &= \hat{\tau}_{SO(4)}^{(2)}|B\rangle|S\rangle = \frac{1}{6}A_2 + \frac{1}{6}A_3, \\ \hat{\tau}_{SO(4)}^{(2)}|S\rangle|S\rangle &= \frac{11}{18}A_2 - \frac{1}{18}A_3, \\ \hat{\tau}_{SO(4)}^{(2)}|B\rangle|\mathbb{1}\rangle &= \hat{\tau}_{SO(4)}^{(2)}|\mathbb{1}\rangle|B\rangle = \frac{1}{36}A_2 + \frac{7}{36}A_3, \\ \hat{\tau}_{SO(4)}^{(2)}|B\rangle|B\rangle &= \frac{-1}{18}A_2 + \frac{11}{18}A_3. \end{aligned}$$

Putting it all together, the previous shows that the P -matrix for the fundamental representation of $O(4)$ is

$$P = \begin{pmatrix} 1 & 0 & 0 & 0 & 0 & 0 & 0 & 0 & 0 \\ 0 & 7/36 & 1/36 & 7/36 & 11/18 & 1/6 & 1/36 & 1/6 & -1/18 \\ 0 & 1/36 & 7/36 & 1/36 & -1/18 & 1/6 & 7/36 & 1/6 & 11/18 \\ 0 & 7/36 & 1/36 & 7/36 & 11/18 & 1/6 & 1/36 & 1/6 & -1/18 \\ 0 & 7/36 & 1/36 & 7/36 & 11/18 & 1/6 & 1/36 & 1/6 & -1/18 \\ 0 & 0 & 0 & 0 & 0 & 0 & 0 & 0 & 0 \\ 0 & 1/36 & 7/36 & 1/36 & -1/18 & 1/6 & 7/36 & 1/6 & 11/18 \\ 0 & 0 & 0 & 0 & 0 & 0 & 0 & 0 & 0 \\ 0 & 1/36 & 7/36 & 1/36 & -1/18 & 1/6 & 7/36 & 1/6 & 11/18 \end{pmatrix}.$$

with P acting on two, three-dimensional vector spaces with basis $\{|\mathbb{1}\rangle, |S\rangle, |B\rangle\}$.